HHS Public Access

Author manuscript

*Neuron*. Author manuscript; available in PMC 2024 September 20.

Published in final edited form as:

*Neuron*. 2023 September 20; 111(18): 2811–2830.e8. doi:10.1016/j.neuron.2023.06.008.

# Mapping the neuroethological signatures of pain, analgesia and recovery in mice

**Manon Bohic**[1,2,†], **Luke A. Pattison**[3,†], **Z. Anissa Jhumka**[4], **Heather Rossi**[4], **Joshua K. Thackray**[6,7], **Matthew Ricci**[8,9], **Nahom Mossazghi**[10,11], **William Foster**[4], **Simon Ogundare**[4], **Colin R. Twomey**[12], **Helen Hilton**[3], **Justin Arnold**[4], **Max A. Tischfield**[1,5,6,7], **Eric A. Yttri**[10,11], **Ewan St. John Smith**[3], **Ishmail Abdus-Saboor**[4,*], **Victoria E. Abraira**[1,2,13,*]

[1]Cell Biology and Neuroscience Department, Rutgers University, The State University of New Jersey, New Brunswick, United States of America

[2]W.M. Keck Center for Collaborative Neuroscience, Rutgers University, The State University of New Jersey, New Brunswick, United States of America

[3]Department of Pharmacology, University of Cambridge, Cambridge, United Kingdom

[4]Zuckerman Mind Brain Behavior Institute and Department of Biological Sciences, Columbia University, New York, New York, United States of America

[5]Child Health Institute of New Jersey, Robert Wood Johnson Medical School

[6]Human Genetics Institute of New Jersey, Rutgers, The State University of New Jersey, Piscataway, NJ, United States of America

[7]Tourette International Collaborative Genetics Study (TIC Genetics)

[8]Data Science Initiative, Brown University, Providence, Rhode Island, United States

[9]School of Computer Science and Engineering, The Hebrew University of Jerusalem, Jerusalem, Israel

[10]Department of Biomedical Engineering, Carnegie Mellon University, Pittsburgh, PA, United States of America

[11]Department of Biological Sciences, Carnegie Mellon University, Pittsburgh, PA, United States of America

[12]Department of Biology, University of Pennsylvania, Philadelphia, PA, United States of America

[13]Lead contact

[*]Corresponding authors: victoria.abraira@rutgers.edu, ia2458@columbia.edu.
[†]These authors contributed equally.

Author Contributions

LAP and MB contributed equally to the work. EStJS, IAS, and VEA conceived the research study. EStJS, IAS, EAY, and VEA designed experiments. LAP performed electrophysiology, $Ca^{2+}$-imaging and immunohistochemistry experiments. MB, LAP, HR, ZAJ, WF and HH performed behavioral experiments. ZAJ, WF, JA, NM, and EAY performed the analysis for PAWS and B-SOiD. MB, MAT, JKT, MR performed the analysis for Motion Sequencing. MB, LAP, IAS, EStJS, and VEA wrote the manuscript. All authors contributed to the editing of the final document.

Competing Interests

The authors declare no conflict of interest with any of the data presented in this article.

## Abstract

Ongoing pain is driven by the activation and modulation of pain-sensing neurons, affecting physiology, motor function, and motivation to engage in certain behaviors. The complexity of the pain state has evaded a comprehensive definition, especially in nonverbal animals. Here in mice, we used site-specific electrophysiology to define key time points corresponding to peripheral sensitivity in acute paw inflammation and chronic knee pain models. Using supervised and unsupervised machine learning tools we uncovered sensory-evoked coping postures unique to each model. Through 3D pose analytics, we identified movement sequences that robustly represent different pain states and found that commonly used analgesics do not return an animal's behavior to a pre-injury state. Instead, these analgesics induce a novel set of spontaneous behaviors that are maintained even after resolution of evoked pain behaviors. Together, these findings reveal previously unidentified neuroethological signatures of pain and analgesia at heightened pain states and during recovery.

### Keywords

Pain; Behavior; Nociception; Electrophysiology; Analgesia; Recovery

## Introduction

Chronic pain represents a major unmet health burden worldwide. Heightened nociception immediately after injury is protective, serving to promote repair and recovery[1,2]. However, during chronic inflammatory diseases, such as rheumatoid arthritis, or following tissue damage and degradation, as seen in osteoarthritis, prolonged periods of heightened nociception do not confer biological advantages, but rather unmitigated suffering. Despite this, approved therapeutic options for treating ongoing pain are often inadequate or accompanied by undesirable side effects[3–5]. The need for safer, more efficacious analgesics is thus paramount; development of such drugs is dependent upon a greater understanding of the mechanisms and complexities underlying pain.

Preclinical models of pain in rodents are often used as an entry point in the search for novel analgesics. The underlying causes of pain, either inflammation or tissue damage, often cause molecular changes culminating in sensitization of neurons which can be identified and probed in these models[6,7]. Inflammatory pain can be modeled by intraplantar injection of compounds such as carrageenan into the paw, which induces robust edema and heightened sensitivity to both thermal and mechanical stimuli[8–10]. Alongside the carrageenan model, other models of pain are perhaps more translationally relevant, recapitulating more clinical features of human pain conditions. For instance, intra-articular injection of monoiodoacetate (MIA) results in a similar pathology to knee osteoarthritis (OA): a transient inflammatory response ensues as MIA causes chondrocyte death which preludes degeneration of the joint space[11]. Human OA patients often describe ongoing, dull, aching pain that is punctuated by sharp pain, which becomes more frequent over time[12]. However, behavioral markers of heightened nociception during a disease state in non-verbal rodents are commonly limited to changes in weight-bearing, locomotion and hypersensitivity to mechanical and thermal stimuli[13]. To date, studies utilizing both the carrageenan and the MIA OA models have

heavily relied on histological analyses and sensory-evoked pain behavior assays to assess the efficacy of therapeutic agents[10,14–16]. With this rather limited level of characterization of such a complex neuroethological state as pain, what prominent features of pain in rodents might have gone undetected? Pain is encompassed by changes at the molecular and cellular levels, which feed through the nociceptive system to encode highly nuanced behavioral signatures. Therefore, to fully understand and measure pain, and assess novel targets for therapeutic intervention, a multidisciplinary approach is needed.

The peripheral nervous system detects environmental cues ranging from the pleasant to the harmful, feeding electrical signals into the central nervous system where appropriate and complex behaviors are elicited. Within the peripheral nervous system, nociceptors are the cardinal drivers of pain, with numerous studies demonstrating greater excitability of sensory neurons following exposure to inflammatory mediators[17]. Retrograde tracers permit identification of the neurons innervating a particular area of the body, thus enabling greater resolution of functional and molecular changes by focusing on the cells projecting to the afflicted area[18]. Traditional methods for studying pain behavior in rodents rely often on evoked pain measures, whereby the degree of pain experienced is inferred from the latency to respond to sensory-evoked stimuli. However, such approaches do not fully capture the nature or assessment of pain in humans and are associated with issues of inherent variability when used by different groups and the potential for experimenter bias[19,20]. Thus, more objective and comprehensive tools to study animal behavior are necessary. Recent advances in computer vision and machine learning have led to the development of more unbiased techniques to monitor evoked animal response such as PAWS (Pain Assessment at Withdrawal Speed)[21] and B-SOiD (Behavioral Segmentation of Open-Field in DeepLabCut[22])[23]. Both techniques can take advantage of high-frame rate videography to detect subtle micro-movements animals perform in response to innocuous or noxious stimulation, followed by analysis of rich data sets by supervised or unsupervised machine learning algorithms. MoSeq (Motion Sequencing) represents a complementary technology where 3D vision is applied to observe an animal's spontaneous behavior[24–26]. Following open-field spontaneous behavior, post-hoc analysis via unsupervised machine learning allows for the extraction of the dozens of motion sequences or modules that make up mouse body language[26]. The overall goal of the current study is to combine such approaches to trace nociception from its sensory encoding to the complex pain behaviors arising from carrageenan-induced inflammation and MIA-induced knee deterioration, providing multidimensional analyses to uncover novel features that define pain progression, analgesia and recovery in mice.

We utilize PAWS, B-SOiD and MoSeq, alongside whole-cell electrophysiology to provide rich mapping of the neuroethological progression of pain following injection of carrageenan or MIA. We observe increased excitability of sensory neurons innervating the site of carrageenan-induced inflammation, which shows signs of recovery within 24 hours. In line with the progressive nature of the model, hyperexcitability of knee-innervating sensory neurons increased with time following injection of MIA to the joint. The thorough analysis permitted by high-speed videography revealed unique paw guarding behaviors in response to application of innocuous vs noxious stimuli. Through computer vision coupled to machine learning, we uncover strings of spontaneous behavioral syllables representative

of pain and pain relief states in freely moving mice, as well as behavioral modulation following administration of analgesics in the absence of injury. Importantly, we demonstrate that while commonly used analgesics can reverse hypersensitivity to noxious stimuli, the pharmacobehavioral space occupied by animals receiving analgesics does not represent a true return to basal conditions. Taken together, our results have major implications on traditional approaches to test the clinical efficacy of new analgesics and evaluate recovery.

## Results

### Carrageenan- and MIA-induced pain alter ethological and evoked behavior alongside changes in sensory neuron excitability across distinct timescales.

The activation and sensitization of sensory neurons innervating injured tissue represent the first steps in the transmission of pain[27]. Neuronal sensitization can trigger long lasting molecular and synaptic changes in peripheral and central circuits[28–30]. How these cellular changes align with behavior is central to understanding, quantifying and treating pain.

To first identify the time points that punctuate the development of injury-induced pain behaviors, we characterized the functional and molecular changes of sensory neurons that innervate injured tissue across time using two rodent pain models. First, the carrageenan model of localized pain because of its widespread use as an inflammatory pain model in rodents and the reversible nature of the injury to study pain progression, analgesia and recovery[31,32]. Second, the monoiodoacetate (MIA) model of knee osteoarthritis (OA), which, like the human condition, involves cartilage degeneration as the first step in irreversible joint damage and inflammation, and can be used to explore pain progression and analgesia[11]. Carrageenan injection into the paw results in swelling of the whole paw and ankle at 4- and 24-hours post-injection[33] (Fig. 1A, C, D and Fig. S1). Traditional measures of pain behavior revealed that the time animals spent rearing, an ethological explorative stance, was reduced 4-hours post-injection, but had recovered as early as 24-hours (Fig. 1G). However, measuring paw withdrawal latency in response to heat with the Hargreaves test, one of the most commonly used assays to measure hypersensitivity following inflammation[34], showed hypersensitivity at both 4- and 24-hours (Fig. 1H). In the OA model, swelling of the knee was observed 3-days after injection of MIA into the joint space and persisted at 10-days post-injection, when histological analysis of knee joints also revealed a loss of cartilage, a key clinical feature of the human osteoarthritis (Fig. 1B, E and F). A significant decrease in rearing behavior, as well as hypersensitivity to the application of mechanical pressure at the site of injury were observed for both time points, with responses at 3- and 10-days being indistinguishable in both assays (Fig. 1I and J). These findings highlight an apparent discrepancy between the progression of reflexive vs spontaneous pain behaviors after carrageenan paw injection, while the dynamic range of current assays cannot differentiate multiple time points of pain progression as the knee joint continues to deteriorate after MIA injection. This suggests that current behavioral readouts testing both reflexive and ongoing pain behaviors are not always sufficient to efficiently track pain progression in rodents.

To better understand whether the apparent behavioral presentation of pain in these two models correlates with neurophysiological changes at the site of injury, we used the

retrograde tracer Fast Blue[18,35] to study the properties of dorsal root ganglion (DRG) sensory neurons specifically innervating the hind paw or knee (Fig 1 K–N). Analysis of cell body diameters revealed the Fast Blue positive populations of hind paw- and knee-innervating sensory neurons resembled the natural distribution of all lumbar DRG neurons (Fig S1). Electrophysiological characterization 4-hours following carrageenan-induced inflammation revealed increased excitability of ipsilateral hind paw sensory neurons, evident from the reduced rheobase, more depolarized resting membrane potential and increased macroscopic voltage-gated inward currents (Fig. 1L, O, Fig S1), suggesting the rapid onset of peripheral sensitization correlating with the peak of physical inflammation at the paw (Fig. 1A, C). At 24-hours, as inflammation begins to subside, and inflammatory mediators decline[36], the degree of excitability also declined to match that of the contralateral side (Fig. 1E, Fig. S1). Increased excitability was also observed for ipsilateral knee sensory neurons 3-days post-injection of MIA (Fig. 1Q). In line with the continued knee deterioration of this more chronic model, ipsilateral neuronal hyperexcitability was maintained at 10-days post-injection of MIA (Fig. 1Q). Moreover, at 10-days post-injection of MIA, a higher proportion of ipsilateral knee-innervating sensory neurons fired multiple action potentials when stimulated at a suprathreshold, an effect not seen at 3-days post MIA-injection, or for either time point tested in the carrageenan inflammatory pain model (Fig. 1P–R). No other differences were observed between ipsilateral or contralateral neurons for either pain model or time point in terms of intrinsic or active electrophysiology properties (Tables 1–2, Fig S1). To further demonstrate that injury affects the sensory biology of nociceptors at the physiological and molecular level in our pain models, expression of TRPV1, an ion channel involved in the detection of noxious heat and marker of nociceptive neurons[37–40], was examined using immunohistochemistry and $Ca^{2+}$ imaging. These experiments revealed that a higher proportion of ipsilateral hind paw sensory neurons expressed TRPV1 compared to the contralateral side 24-hours post-inflammation (Fig S1). A greater proportion of ipsilateral knee-innervating neurons were also found to be sensitive to capsaicin in the MIA model (Fig S1).

Our results demonstrate that both paw inflammation and knee injury have profound effects on sensory neuron biology. Although the excitability of sensory neurons is mostly affected during early time points following inflammatory insult, longer-lasting molecular changes are seen later on. Such findings demonstrate that 4- and 24-hours after an inflammatory insult are informative time points to study the transition from acute changes to peripheral neuron excitability to longer-lasting molecular changes that feed into the central nervous system and ongoing inflammatory pain. Meanwhile, MIA-induced irreversible knee deterioration provides a clinically relevant model of chronic pain with worsening anatomical signs of knee osteoarthritis from 3- to 10-days, that coincide with ever greater sensory neuron hyperexcitability. Taken together our results highlight key biological changes within the peripheral nervous system that punctuate pain progression over time. However, the cellular changes observed do not appear to correlate with current binary algesiometric assays for sensory evoked and spontaneous behavior, indicating that these approaches have insufficient dynamic range to resolve the time course of injury and healing.

### High-speed videography of sensory-evoked reflexes resolve injury progression and differentiate allodynia from hyperalgesia.

To increase the dynamic range of sensory-evoked behavior assays we used high-speed videography to break down paw withdrawal to sensory stimuli into sub-second movements within groups of short-latency reflexive features at stimulus onset vs longer-latency affective behavioral features that occur after paw withdrawal and before paw placement back to the surface[21,41] (Fig. 2A, B). Mechanical hypersensitivity is a common symptom of inflammatory pain, presenting itself as either allodynia, when innocuous stimuli become painful[42–44], or as hyperalgesia, when there is an increased sensitivity to noxious stimuli[45,46]. While allodynia and hyperalgesia can easily be assessed in the clinic[47,48], differentiating them in non-verbal animals is a challenge[49,50]. Thus, with high-speed videography we recorded the animal's response to both innocuous (brush) and noxious (pinprick) stimuli. With this strategy we did not observe a significant change in reflexive behavior responses (paw height, velocity and distance) to innocuous or noxious stimulation following carrageenan injection (Fig. S2). However, coping behaviors (paw shaking and paw guarding) associated with affective behaviors, are more dynamically regulated at 4- vs 24-hours post-injury in response to brush and pinprick (Fig. 2C, D). Indeed, while paw shaking and guarding duration evoked by brush are significantly increased at 4-hours, paw guarding duration evoked by pinprick is upregulated at both the 4- and 24-hour time points (Fig. 2D). Injury can sometimes cause not only primary but also secondary hypersensitivity, i.e. hypersensitivity at a secondary site outside of the site of injury[51–53]. We therefore assessed if high-speed videography could detect secondary hypersensitivity at the paw after knee injury in the OA model. Interestingly, MIA knee injection did not seem to affect reflexive features in response to brush or pinprick stimulation (Fig. 2E) but it increased affective coping behavior in response to innocuous stimulation (guarding duration, Fig. 2F) at 10-days post-MIA compared to baseline. Thus, we capture here the presence of secondary allodynia at the hind paw after MIA knee injection[54,55].

To further differentiate the affective behavioral signatures of hypersensitivity at the primary site of injury, including signatures identified above specific to noxious vs innocuous stimuli[56,57], we employed a recently developed unsupervised machine learning approach to parse spatiotemporal patterns in paw position data (B-SOiD[23]) at 4- vs 24-hours post-carrageenan. For accurate comparison, we used the same high speed behavioral data collected in Fig. 2A–F. As inputs, we used two positions within the hind paw and two reference points as identified with the deep neural network DeepLabCut (see Methods). B-SOiD then identified and extracted unique clusters of conserved motor responses to these stimuli (Fig. 2G; categorical names were assigned to clusters post hoc; all data shown). We found eleven sub-action clusters across stimulation contexts. These behaviors and distributions were similar to those observed by our top-down supervised approach (Fig. 2A–F), but with clear distinctions. Notably, B-SOiD extracted a combination of two unique guarding types (i.e. angled vs flat guard, see Supplemental videos) that was different based on the foot stimulus presented (Fig. 2H–I). These phenotypes were distinct from each other in both height and foot posture. Mice exhibited an upregulation of the angled guard (characterized post-hoc as paw lifted and perpendicular to the surface, Fig. 2J) in response to brushing at 4-hours post-carrageenan compared to baseline occurrence ($p<3e-12$, Fisher's

exact test). Conversely, the flat guard appeared only in response to pinprick stimulation after injury (paw lifted and parallel to the surface), likely associated specifically with hyperalgesia[58] (Fig. 2I, K). This guard type was the dominant action induced by noxious stimulation after carrageenan-induced inflammation ($p<1e-20$ for either 4- and 24-hours post-injection time point compared to baseline occurrence, Fisher's exact test). However, the display of the flat guard was absent in all baseline samples, as well as across brush conditions. Thus, the angled guard coping response alone is characteristic of allodynic behavior post-carrageenan, while the flat guard is specific to hyperalgesia. We also note that the combined performance of these two specific behaviors identified through unsupervised discovery agrees with the temporal profile of general paw guarding durations identified with our supervised approach as time progresses (Fig. 2D). Additionally, a lift-to-hover pattern (e.g. successive, alternating paw lifts (green) and hovering (yellow), Fig. 2H–I) was identified as a behavioral combination analogous to a hind paw shake (see videos in Supplemental Information). This lift-to-hover pattern was observed at baseline, but became repeated and extended after injury, particularly with the brush stimulus (brush – 4-hours vs baseline: $p<4e-9$, 24-hours vs baseline: $p<2e-15$; Fig. 2H).

Altogether, our approach finely measured the transition in inflammatory-induced sensitization at 4- and 24-hours after paw inflammation, and secondary paw allodynia and hyperalgesia after knee injury. This highlights the importance of affective behavioral biomarkers as representations of inflammatory pain independent of the site of injury. We find that inflammatory pain specifically alters the responses to mechanical stimuli such that defensive coping behaviors are more frequent. Interestingly, we show that mechanical allodynia (e.g. hypersensitivity to innocuous stimuli) appears as early as 4-hours post-carrageenan and 3-days post-MIA injection while mechanical hyperalgesia (e.g. hypersensitivity to painful stimuli) is most upregulated at 24-hours. To our knowledge this is the first evidence of a robust and generalizable sensory-evoked behavior feature that distinguishes mechanical allodynia vs mechanical hyperalgesia in rodents.

## Ethological approach to movement-evoked spontaneous measures of inflammatory pain

Sensory-evoked responses alone do not accurately reflect the most common symptoms experienced by chronic pain patients[59]. Intuitively, we know that an injured knee can change the way we walk, abdominal pain can change the way we stand, and chronic pain in general can change the way we interact with our environment as well as each other. Movement-evoked and spontaneous pain are significantly greater and a far more common clinical problem than tactile hypersensitivities[60–62]. Our findings that ethological behaviors can also define pain progression over time (Fig. 1G, I) prompted us to explore unbiased approaches to scoring behaviors in freely moving mice at 4- vs 24-hours post-carrageenan paw injection and at 3- vs 10-days post-MIA knee injection. To detect, measure and scale behavior in freely moving animals, we used time-of-flight infrared cameras to detect mouse body contours, depth and movement during 20-min long sessions. We then applied 3D pose analysis using unsupervised machine learning (Motion Sequencing or MoSeq)[24,26] to identify sets of sub-seconds long movements (a.k.a. "modules") that best categorize spontaneous behavior in models of paw inflammation and knee osteoarthritis (Fig. 3A). Linear Discriminant Analysis (LDA) of module usage shows the global transformation of

spontaneous behavior as it adapts over time to the injury (Fig. 3B–C). The progressive transformation we uncover here resolves the discrepancy between the punctual change in rearing behavior as measured by traditional approaches at 4-hours (Fig. 1G) and the ongoing evoked pain at 4- and 24-hours (Fig. 1H) in carrageenan-induced paw inflammation. It also allows us to capture the progression of pain between early and later time points, which Is sometimes indistinguishable with more traditional sensory evoked assays, both for paw and knee pain (Table S1).

To identify ethologically meaningful modules representative of spontaneous and movement-evoked pain, we classified the 69 identified modules as belonging to one of four types of behavior: locomotion, grooming, pausing and rearing (Table S1). We found that all four types of behaviors were affected as a result of paw inflammation and knee osteoarthritis (Table S1, Fig. S3). In accordance with traditional measures showing a decrease in rearing behavior at 4-hours after carrageenan paw injection and at 3- and 10-days after MIA knee injection (Fig. 1G, I), we found that the usage of rearing modules is downregulated (e.g. downregulated rearing module 36, Fig. 3G post-carrageenan and rearing module 18, Fig. 3J post-MIA). However, we found a prolonged impact of pain on rearing behaviors also at 24-hours post-carrageenan injection (Fig. 3G, Table S1). This result suggests that rearing actually remains painful for animals at 24-hours, highlighting ongoing pain often observed following inflammation and sometimes missed by traditional approaches (Fig. 1G). Interestingly, we also found upregulated pausing and grooming modules during ongoing pain in both pain models (e.g. upregulated pausing module 4, Fig. 3H post-carrageenan and Fig. 3K post-MIA, and upregulated grooming modules 59, Fig. 3I post-carrageenan and 60, Fig. 3L post-MIA, pausing modules: 4, 49 post-carrageenan injection, 3, 4, 17, 49, 53 post-MIA injection, Fig. S3). Thus, inflammatory pain localized in the paw and in the knee induces a mosaic of behavioral changes that we can resolve with 3D pose estimation analysis. Moreover, we could capture different sets of modules affected at 4- vs 24-hours post-carrageenan and 3- vs 10-days post-MIA, as well as when comparing paw vs knee pain (Table S1). Therefore, spontaneous behavior as captured by 3D pose estimation informs pain progression in a complementary manner to sensory evoked assays and can discriminate between pain of different etiology.

Altogether, we find that 5 out of 69 modules are differentially regulated at 4- vs 24-hours post-carrageenan and 4 out of 69 at 3- vs 10-days post-MIA. We propose that these modules represent a cohort of sensitive behavioral biomarkers of ongoing pain, central to understanding the neuronal networks driving pain progression over time. For example, resolving precisely how these specific spontaneous pain signatures correlate to neuronal activity driving plasticity changes from peripheral to central mechanisms is crucial to targeted analgesic development.

### Gabapentin improves evoked and spontaneous signatures of osteoarthritis knee pain while meloxicam relieves tactile hyperalgesia following inflammation.

To validate both sensory-reflexive (Fig. 2) and spontaneous (Fig. 3) pain behavioral biomarkers, we explored the effects of drugs commonly used in veterinary and human medicine for inflammation and/or pain management. We aimed to test pain relief in

carrageenan-induced pain with the anti-inflammatory drug meloxicam and MIA-induced osteoarthritis pain with gabapentin at 24-hours and 10-days respectively (Fig. 4A–B). Meloxicam and gabapentin are commonly used to relieve inflammation and pain in rodents, dogs, cats and humans[63–72]. At 22-hours post-carrageenan paw injection and 10-days post-MIA knee injection respectively, we injected mice with either saline or meloxicam (for carrageenan-induced pain) or gabapentin (for MIA-induced pain) intraperitoneally. We then assessed carrageenan-induced plantar heat hypersensitivity with Hargreaves (Fig. 4C), MIA-induced knee hypersensitivity to mechanical pressure (Fig. 4D), sensory-reflexive responses with high-speed videography (Fig. 4E–F), and spontaneous behaviors with 3D pose dynamic analysis (Fig. 4G–L). As expected, we found meloxicam reduced carrageenan-induced heat hypersensitivity (Fig. 4C) and gabapentin reduced MIA-induced knee pressure hypersensitivity (Fig. 4D). We then tested paw sensory-reflexive responses with high-speed videography and machine learning (Fig.4E–F). While we could not capture gabapentin-mediated analgesia at the secondary site of hypersensitivity (paw) post-MIA knee injection (Fig. 4E), we found that meloxicam alleviated the carrageenan-induced hyperalgesic response to pinprick typically observed at 24-hours (Fig. 4F). Combined with the hyperexcitability of injury-innervating neurons observed at 4- but not 24-hours (Fig. 1E), this suggests that prolonged inflammation results in sensitization of central circuits that drive tactile hyperalgesia, and that meloxicam can target this secondary effect of inflammation to blunt this behavior.

Next, we assessed the effects of meloxicam and gabapentin on identified spontaneous signatures of pain (Fig. 4). We found that meloxicam reinforced the shift in spontaneous behavior we observed in animals in carrageenan-induced pain (Table S1, Fig. S4). On a global scale we observed a further reduction in locomotion and rearing modules, and elevated pausing and grooming modules (Fig. 4G, H, rearing #15 and #60 grooming, Table S1). In total we observed 23 deregulated modules at the analgesic vs baseline state (i.e., 24-hours+meloxicam vs baseline+saline) compared to only 8 deregulated modules between baseline and pain states (i.e., baseline+saline vs 24-hours+saline). Gabapentin administered to animals at 10-days post-MIA knee injection showed a different shift in behavioral profile. Most notably, gabapentin administration at 10-days post-MIA induced an improvement in usage of locomotion and rearing modules compared to animals that received saline (Fig. 4J, K, rearing #18 and #57 locomotion). This suggests beneficial effects of gabapentin on spontaneous signatures of pain. Consistent with individual module results, the behavior state maps drawn by LDA of module usage show that the spontaneous behavior of animals in pain that received an analgesic is different from that of animals pre-injury and animals in pain that received saline (Fig. 4I, green baseline+saline, pink 24-hours+saline, dark blue 24-hours+meloxicam, Fig. 4L, green baseline+saline, red 10-days, darker blue 10-days+gabapentin). For example, while the point clouds in Figure 4I and 4L do show some overlap between conditions, cohorts can be distinguished by their module usage, which we quantified by computing the F1 of the LDA in predicting the condition of the held-out animals (30% training set, 70% test set or held-out animals; F1-scores on the test set: CAR bsl+saline = 0.57, CAR bsl+meloxicam = 0.50, CAR 4h = 0.67, CAR 24h+saline = 0, CAR 24h+meloxicam = 0.40, overall model accuracy = 0.50, better than “pure-chance” = 0.20 and randomized data). For accuracy, we report F1, the harmonic mean of precision

and recall. We thus conclude that meloxicam and gabapentin resolve sensory-evoked aspects of pain in mice, but do not bring spontaneous behavior back to a pre-injury state (Fig. 4I, L, Fig. S4). This unexpected finding led us to question whether they might also alter baseline behavior in the absence of pain. Our analysis demonstrates that both meloxicam and gabapentin indeed affect spontaneous behavior even when administered in uninjured animals (Fig. 4G–L, Fig. S4). While this is to be expected for gabapentin, a drug with known sedative effects via reduced neuronal excitability[73–75], this is more surprising for meloxicam which acts by reducing pro-inflammatory, injury-induced prostaglandin production[36,76].

## Higher order behavioral sequences predict pain and analgesic states in rodents

While sub-second movement-evoked pain signatures can be resolved at a single module-transition analysis (Fig.3), ongoing pain signatures necessitate a different analytical approach, one that can describe the structure of behavior over a longer time scale (i.e., over multiple modules and transitions). To quantitatively represent longer behavioral sequences, we first asked whether analysis of transition probabilities can be used to more accurately describe ongoing pain signatures. Thus, we calculated transition probabilities by counting the total number of occurrences where module A is followed by module B, for all modules. In this case, we used a Sankey diagram to represent transition probabilities between incoming and outgoing modules based on root module 18, a rear for which usage decreases as MIA-induced pain progresses and which is rescued by gabapentin administration (Table S1, Fig. S5). We find that most sequences are stable across time, for example, 18 can be preceded by 1, forward locomotion, and followed by 11, full rear, at baseline, 3-days and 10-days after MIA knee injection and even after administration of gabapentin (blue, Fig. S5). Though the probability of this full rear following 18 decreases across time as mice perform less full rears when in pain (Table S1). Instead, we see new sequences 1>18>2 or 1>18>20 appear whereby instead of proceeding to a full rear, the mouse sometimes pauses (2) or comes down from the rear (20) when it is in an ongoing pain state at 10-days (yellow, Fig. S5). We hypothesized that these unique novel sequences could be representative and discriminative of various pain states (4- vs 24-hours post-carrageenan and 3-days vs 10-days post-MIA).

If we compare the analysis of spontaneous behavior to deciphering a new language, module usage informs us on word frequency, which holds only limited meaning as to the state of the animal. However, extracting sequences of modules, akin to deciphering the meaning of entire sentences[77,78], might provide a better representation of ongoing pain states. To test this model, we applied standard sequence classification techniques of natural language processing[79] to extract sets of modules which best represent a particular experimental group (carrageenan: baseline + saline, baseline + meloxicam, 4-hours post-carrageenan injection, 24-hour post-carrageenan injection + saline, or 24-hour post-carrageenan injection + meloxicam; MIA: baseline + saline, baseline + gabapentin, 3-days post-MIA injection, 10-days post-MIA injection + saline, 10-days post-MIA injection + gabapentin). These methods embed long sequences (i.e., the raw sequencing data produced by one animal) in a representational space where sequences having similar co-occurrence structure (pairs of modules, triples of modules, etc.) tend to cluster. Consequently, these embeddings depend on contextual information[80] which is absent in module usage data and potentially

more powerful than first order transition probabilities (see Materials and Methods, Learned Embeddings of Module Sequences). To evaluate the relative predictive powers of usages vs first order transition probabilities vs learned embeddings, we trained three multinomial logistic regression classifiers to predict experimental groups from each type of representation (see Materials and Methods, Classifier Analysis of Animal Representations). Context-dependent, learned embeddings (Fig. S5) were substantially more predictive of experimental groups than raw usages or transition probabilities on hold-out test data (.223 and .492 F1 for raw usages for carrageenan and MIA resp.; .257 and 406 F1 for transition probabilities for carrageenan and MIA resp.; .538 and .781 F1 for learned embeddings for carrageenan and MIA resp.).

Learned embeddings now provide us with the means to identify precise behavioral sequences that characterize different pain states. To apply this finding, we adapted standard module co-location metrics[80] to detect 2-, 3- and 4-long modules that characterized each of the experimental conditions (Fig. 5, Table S1). These methods proceed by recursively agglomerating neighboring modules into higher-order units according to whether the higher-order unit appears significantly more than its constituents in the full sequence. This allowed us to identify sequences of spontaneous behavior most representative of the various mouse internal states we probe here such as pre-injury (baseline + saline), acute pain (4-hours post-carrageenan), adaptation to pain (10-days post-MIA knee injection), effect of a common analgesic drug on ongoing pain (10-days post-MIA knee injection + gabapentin) (Table S1). Mainly we found that sequences comprising grooming and pausing behavior are most representative of early pain states (38>14>23, 64>56>41 at 4-hours post-carrageenan, 40>4>40>19, 64>56>41 at 3-days post-MIA) (Table S1). Moreover, mice injected with MIA adapt their behavior between 3- and 10-days after knee MIA injection whereby slow explorative sequences best characterize their behavior at 3-days, whereas at 10-days sequences combining half-rears and exploratory behavior appear. Finally, meloxicam administration (24-hours post-carrageenan + meloxicam) seems to abolish sequences of escape behavior exhibited by mice at 4- and 24-hours.

We then ablated these specific behavior sequences (constituting only 0.535 % and 0.678 % of the total modules in the MIA and carrageenan conditions respectively) by replacing them with random modules to re-learn embeddings on these ablated sequences. Despite removing only a small portion of the total modules, this procedure resulted in an average drop in test-data classifier F1 of 0.166 +/− .015 for the MIA condition and 0.237 +/− .075 for the carrageenan condition, placing it within a standard deviation from the performance of the transition representation (Fig. 5E, F). In contrast, when the same number of random modules were ablated, testing F1 score was essentially the same (decreasing only by .011 in the MIA condition and increasing very slightly by .002 in the carrageenan condition (Fig. 5E, F). We take this quantitative result as a proof of concept not only that complex behaviors beyond usages and transitions characterize different pain states but also that these complex behaviors can be detected using standard sequence representation methods from machine learning.

In conclusion, we have identified the learned embeddings method as a crucial tool to extract biologically meaningful data from rich and complex behavior datasets. This allowed us to

uncover specific behavioral signatures of spontaneous pain as well as quantify the efficacy and side-effects of analgesics.

## Spontaneous behavior remains affected long after inflammation-induced sensory-evoked hypersensitivity has resolved

We found that pain relief from sensory-evoked hypersensitivity, usually assumed to equal analgesia, does not coincide with a return to pre-injury spontaneous behavior (Fig. 4). To investigate whether spontaneous behavior ever returns to a pre-injury state, we first assessed sensory-evoked thermal sensitivity with Hargreaves and mechanical sensitivity with von Frey at baseline and at 4-hours, 24-hours, 3-days, 6-days and 14-days post-carrageenan paw injection (Fig. 6A). We found by 6-days post-carrageenan injection thermal and mechanical sensitivity were similar to baseline (Fig. 6B, C). We next used 3D pose analysis to probe variations in spontaneous behavior at those time points where sensory-evoked hypersensitivity has resolved. We were surprised to find the usage of 24 and 17 modules out of 69 were still deregulated at 6- and 14-days post-carrageenan injection respectively compared to baseline (Table S1, Fig. 6D, purple vs green). Of the 13 syllable usages which were deregulated in pain (Table S1, Fig. S3), we found 6 modules which showed a return to pre-injury: 2 rearing modules, 2 grooming modules and 2 locomotion modules (e.g. rear against the wall, module 46, Fig. 6E and grooming, module 59, Fig. 6F, Fig. S6). However, other rearing modules were still downregulated (5 out of 23 total rearing modules, example module 15, Fig. 6G) and pausing modules were still upregulated (6 out of 16 total pausing modules, example module 34, Fig. 6H, Fig. S6) at 14-days after carrageenan injection. To control for habituation-induced changes in module usage, we compared the modules affected after carrageenan injection with modules affected after saline injection in the paw and 3D imaging following the same schedule (Fig. S6). Importantly, the modules that might be representative of habituation, as identified by comparing baseline and 6-days post-saline injection, and baseline and 14-days post-saline injection, are overall different from the modules that are deregulated at 6- and 14-days after carrageenan injection. Specifically, out of 24 modules deregulated at 6-days after carrageenan injection, only 5 are also deregulated in the control saline group, and out of the 17 modules deregulated 14-days after carrageenan injection, only 4 are also deregulated in the control saline group. Thus, we believe that most of the 24 and 17-set of modules identified at 6- and 14-days post-carrageenan injection in this manuscript are likely to represent longer-term pain-related changes in spontaneous behavior. Of note, the spontaneous behavior of mice that had received meloxicam at 24-hours was very stable at 6- and 14-days post-carrageenan (Fig. 6I). Strikingly, this was not the case for mice that did not receive meloxicam at 24-hours, where we could see an ongoing change in spontaneous behavior between 6- and 14-days after injury (Fig. 6J). While it remains unclear if mice regain full usage of rearing behaviors at a later time point, it is interesting to observe a module-usage stabilizing effect of meloxicam, a drug with an elimination half-life of ~20-hours[81], after just one administration. Future studies will need to probe whether this effect is beneficial to other recovery metrics like depression and anxiety.

In conclusion, our methods demonstrate a divergence in the timeline for recovery of sensory-evoked vs spontaneous behaviors from inflammatory pain, suggesting that the

neuroinflammatory mechanisms and neural pathways underlying these two aspects of injury-induced pain are different.

## Discussion

Using two different rodent pain models, we provide a holistic assessment of pain behaviors, analgesia and recovery in the mouse that is correlated to key changes in neuronal excitability. With videography across timescales followed by unbiased analyses using machine learning, we identify evoked and spontaneous behaviors of inflammatory pain previously undetected with traditional methods. Profiling sensory neurons directly innervating the site of injury revealed that changes in neuronal excitability initiate inflammatory pain, and that persistent pain is driven by molecular changes[27,82,83]. We determined that while widely used pain management strategies (meloxicam in veterinary medicine and gabapentin in human medicine) might provide relief from tactile hypersensitivities, they rarely equate to a return to a pre-injury state when it comes to spontaneous ethological signatures of pain. Finally, recovery of evoked and spontaneous behaviors after injury does not seem to follow the same timeline, suggesting different neural pathways underlie the evoked and spontaneous aspects of the pain experience. Taken together, these data provide a new multidisciplinary approach for arraying highly dimensional pain behavior datasets and offer a new experimental roadmap for assaying analgesic efficacy and recovery in preclinical rodent models.

### Resolving pain behaviors across time

A single injection of carrageenan produces localized inflammation, which starts resolving within a day, but noxious sensations can persist for days. Here, we demonstrate higher excitability of sensory neurons innervating the inflamed hind paw after 4-hours of inflammation. This rapid onset of hyperexcitability, as well as the pain relief mediated by meloxicam, point to the involvement of specific molecular mechanisms such as the release of prostaglandin E2 (PGE2)[34,36]. However, our electrophysiological approach shows that sensory neurons innervating the site of inflammation are no longer hyperexcitable 24-hours after inflammation. This suggests that the persistent pain behaviors we observe at the 24-hour time point are likely driven by adaptations of the nociceptive system. Indeed, we show an increase in the number of sensory neurons expressing TRPV1 24-hours after induction of inflammation. Our results show that the status of sensory neurons evolves rapidly with inflammation, with unique changes in the activity and molecular profile of sensory neurons that are punctuated at discrete time points post-injury. This is consistent with recent findings from RNA profiling of sensory neurons in a longer-lasting inflammatory pain model (complete Freund's adjuvant (CFA) paw injection) showing an increase at 48-hours in PGE2 synthase expression in peptidergic nociceptors and TRPV1 in both peptidergic and non-peptidergic nociceptors[84,85].

Knee neuron hyperexcitability increases from 3- to 10-days after MIA knee injection as degeneration of the articular cartilage progresses (Fig. 1F). Additionally, as peripheral nociceptor signaling is maintained, central circuits adapt and the resulting pain experience is due to both peripheral and central sensitization[86], hence behavioral pain signatures should

evolve. However, neither mechanical pressure sensitivity nor traditional assessment of rearing behavior could differentiate the osteoarthritis-like pain experience of rodents at 3- vs 10-days (Fig. 1I–J), again highlighting the limited dynamic range of traditional assays and the need for more global pain assessment. Using computer vision and unsupervised machine learning, we identified unique spontaneous behavior signatures at 3- and 10-days with a different set of rearing modules being downregulated at each time point and an increase in grooming behavior at 10-days, but not at 3-days, post-MIA knee injection. Interestingly, this increased grooming is resolved after gabapentin injection, as well as certain rearing behaviors being restored.

Developing, screening and testing single and combination therapies to treat pain over time requires an ability to differentiate between these critical time points with unique and easily identifiable behavior signatures. With machine learning we can now identify discrete sets of behaviors that correlate with pain of different etiologies, pain progression and its relief, or lack thereof.

## Supervised and unsupervised learning approaches to scale sensory-reflexive paw withdrawal behaviors can distinguish hyperalgesia and allodynia

Using the 4- and 24-hour time points to anchor our sensory-reflexive behavioral studies, we show that the early onset of paw withdrawal behaviors in response to stimulation at the primary site of injury are unaltered over time (paw speed and height, Fig. 2). However, we observe an upregulation of defensive coping behaviors like paw guarding as pain progresses from 4- to 24-hours. This is consistent with recent work demonstrating that supraspinal brain structures like the parabrachial nucleus of the brainstem and the central and basolateral amygdala coordinate more complex defensive coping behaviors, like attendance to the stimulated area and escape behavior, at longer time scales[87–90]. Taken together, our results show a distinction between strictly reflexive and supraspinal mediated coping behavioral responses to sensory stimulation under pathophysiological conditions, that can be distinguished across time and are specific to different sensory modalities. In addition, our work shows identifiable variations in guarding responses to innocuous and noxious stimuli. To our knowledge, this is the first demonstration that differences in paw guarding behaviors are specific to a given mechanosensory stimulation, finally allowing for the nuanced distinction between allodynia and hyperalgesia in preclinical animal models.

## 3D pose estimation establishes spontaneous pain signatures and redefines the relationship between analgesia and recovery in preclinical rodent models

While sensory-evoked behavior measurements are necessary for the estimation of rodent pain[91], our addition of 3D pose estimation to scale spontaneous pain behaviors provides a more rounded and unbiased picture of the overall rodent pain state (sensory-discriminative, affective-motivational, and cognitive-evaluative components[59]), which more accurately resembles our own lived pain experiences. Our 3D pose estimation studies uncover two distinct trends in how ongoing pain affects general behavior. First, we show that mice differentially use unique micro-movements at 4- vs 24-hours after carrageenan compared to pre-injury (4 and 8 modules deregulated at 4- and 24-hours respectively), suggesting a qualitatively different pain experience at 24-hours. Second, we find a parallel trend that

follows a U-shaped curve where the usage of certain movements is most affected during the acute phase and tends to revert to pre-injury levels at 24-hours. This second trend suggests an adaptation of motor behavior to pain. Importantly, those two parallel types of adaptation of spontaneous behavior to ongoing pain are recapitulated in the MIA-induced model of knee osteoarthritis whereby a minority of behaviors tend to improve at 10-days, but the majority worsen as cartilage degeneration, bone necrosis and inflammation progress. Unexpectedly, 25% of modules are still deregulated after sensory-evoked carrageenan-induced hypersensitivity has resolved. Indeed, we find that certain types of rearing behavior, mainly full rears, are still less used by mice 14-days after carrageenan paw injection, potentially because they are still painful and/or uncomfortable.

The International Association for the Study of Pain describes pain as both a sensory and an emotional experience[92], with analgesia broadly defined as a lack of pain or an insensitivity to pain. By this current definition an analgesic provides relief from both sensory-evoked and ongoing emotional pain. However, is analgesia a return to a pre-injury state or a different state altogether? Our combined approach shows that each pain state (pre-injury, 4-, 24-hours post-injury, etc.) occupies a unique corner of behavioral space and can be defined by unique sequences of sub-second movements. While meloxicam can relieve mechanical and thermal sensory-reflexive responses, its effect on spontaneous behavior is more subtle as mice injected with either saline or meloxicam at 24-hours post-injury still share common sub-second movements and movement sequences. Thus, our pose estimation results demonstrate that current analgesic treatments for pain are unlikely to revert an animal back to a pre-injury behavioral state. However, the application of combined approaches that can more accurately correlate unique and distinguishable behavior signatures with their underlying pathological mechanisms will drastically improve the translational potential of analgesic drug development from bench-to-bedside.

## Looking towards the future: how should we measure pain and analgesia in rodents?

Here we propose a large array of computational approaches to better define sensory-evoked and spontaneous pain progression from acute to chronic, and identify unbiased markers of analgesic efficacy. The growing number of computational tools available for automated tracking of animal behavior might make it seem difficult to choose the most appropriate one. We discuss here our insights on the advantages and limits of the supervised and unsupervised approaches we used to study two broadly used animal pain models: transient carrageenan-induced inflammatory paw pain and persistent osteoarthritis-like MIA-induced knee pain. First, generally speaking, the nature of the injury model should guide researchers towards the use of sensory-evoked (for example DeepLabCut[22] or SLEAP[93] tracking followed by PAWS[21], B-SOiD[23] analysis of behavior) and/or spontaneous pain tracking (for example 3D imaging from above or below followed by behavior segmentation and analysis using MoSeq[26,94] or B-SOiD). As a general rule, for techniques that produce such fine and granular level of behavior tracking, the design of the experiment and inclusion of control groups is crucial. Here for example, we included a control cohort to monitor habituation-induced changes in module usage with MoSeq (Fig. S6). Furthermore, as highlighted in our study of MIA-induced knee pain, subsecond tracking of paw withdrawal might not be informative of the pain state of the animal when the injury concerns a body part other than

the paw, for example in the case of visceral pain. However, we were able to capture the commonality of global markers of ongoing pain: increased pausing and grooming, decreased rearing, both for paw and knee pain by using 3D imaging and MoSeq. Second, while the sum of all pausing module usages is significantly upregulated at baseline compared to pain states, we do believe it is important and meaningful to also analyze at the specific module level for a variety of reasons. For example, the module level analysis shows more subtle effects of meloxicam administration: one specific pause is significantly downregulated, whereas another type of pause is significantly increased. The granularity generated by such analyses allows the investigator to interrogate on- and off- target effects of drugs which would otherwise be masked by agglomeration, which is the classical approach in human-scored behaviors and pain research. At an ethological level, not all pauses are equal, and humans are poor at correctly classifying these appropriately, which is the benefit of unsupervised approaches such as MoSeq.

Modern machine learning methods tend to work best in the big data regime, where the number of samples is much larger than the number of features. However, ethological data often falls outside this regime, since a sample corresponds to one animal and many-animal experiments are expensive. However, as data collection techniques improve and sample sizes grow, big-data approaches become increasingly feasible. Our setting, with hundreds of samples each with tens of thousands of modules, represents a transitional moment in data scale at which the comparative advantage of traditional vs modern methods is difficult to decide in advance. The current manuscript demonstrates that, while modern methods (e.g. learned embeddings) can achieve better raw prediction than traditional techniques (e.g. LDA), their results are often difficult to interpret, necessitating explanatory workarounds like those which produced the behavior motifs in the Section “Higher order behavioral sequences predict pain and analgesic states in rodents”. Traditional methods, for their part, show the opposite relation between prediction and interpretability. Nevertheless, the direction of the field is clear, and the era of truly big-data ethology will usher in the methods we have begun to explore here.

Our view is that sequence analysis techniques like those we have adapted from natural language processing represent an exciting opportunity for this new era. Importantly, they take advantage of the discrete nature of module data and can incorporate arbitrary timescales, unlike the simple Markovian assumptions underlying the transition representation. Second, new natural language methods based on transformers (e.g. GPT-4[95]) have shown great promise in sequence generation. Although we have not explored generative modeling in this manuscript, we believe that the ability to synthesize new behavioral sequences and indeed new “animals” will have significant theoretical and clinical applications. The development of sequence processing methods for ethology is an important step towards this ability.

## STAR Methods

### RESOURCE AVAILABILITY

**Lead contact—**Further information may be requested from and will be provided by the corresponding author Victoria E. Abraira (victoria.abraira@rutgers.edu).

**Material availability—**This study did not generate new unique reagents or mouse lines.

**Data and code availability—**Behavioral and electrophysiological data have been deposited at Zenodo (https://doi.org/10.5281/zenodo.7884191) and are publicly available as of the date of publication. Software and code used in this manuscript is available from the sources listed in the key resources table, and is publically available as of the date of publication, subject to their individual licenses. Any ad hoc scripts used within this manuscript for plotting have been deposited at Zenodo, in the same repository as, and alongside, the corresponding data. Any additional information required to reanalyze the data reported in this paper is available from the lead contact upon request.

## EXPERIMENTAL MODEL AND STUDY PARTICIPANT DETAILS

**Animals (Rutgers University)—**Wild Type male mice of C57BL/6N background were used for behavioral analyses. All mice were adults between 2 and 4 months. All procedures were approved by the Rutgers University Institutional Animal Care and Use Committee (IACUC; protocol #: 201702589). C57BL6 mice were purchased from Jackson Laboratories. All animals were habituated to our facility for 2 weeks after delivery before beginning behavioral experiments described below. All mice used in experiments were housed in a regular light cycle room (lights on from 08:00 to 20:00) with food and water available ad libitum. All cages were provided with nestlets to provide enrichment. Animals were co-housed with 4 mice per cage in a large holding room containing approximately 300 cages of mice. 20 μl 3% (w/v) λ-Carrageenan (Sigma-Aldrich) in PBS 1X was injected into the mouse left hind paw using a Hamilton syringe for the carrageenan model of paw inflammation. 10 μl 0.1 mg/μl sodium iodoacetate (VWR) in PBS 1X was injected into the knee joint for the MIA-induced model of knee osteoarthritis. All animals were acclimated to the testing room for an hour prior to testing. For 3D pose imaging, mice were gently placed in the middle of a circular 17” diameter enclosure with 15”-high walls (US Plastics) and allowed to roam freely for 20 minutes while being recorded with the Kinect2 depth-sensing camera. Mice were habituated to the Hargreaves testing chambers for two hours over two days. Thermal hyperalgesia was assessed at baseline and 6- and 26-hours post-carrageenan injection after 3D pose imaging at baseline, 4- and 24-hours post-carrageenan injection. Inflammation was induced while mice were under inhalation anesthesia (2 to 3.5% isoflurane according to mice’s loss of consciousness and anesthetic depth (monitoring of respiratory rate and pattern and responsiveness to toe pinch). Saline or meloxicam (5mg/kg, Henry Schein Animal Health) was injected intraperitoneally 22 hours post carrageenan injection (2 hours before the last 3D pose imaging session).

**Animals (University of Cambridge)—**Wild Type male mice of C57BL/6J background were used for behavioral, electrophysiological and histological analyses. All mice were adults between 2 and 4 months. Experiments performed in Cambridge, UK (dynamic weight bearing, pressure application measurement, electrophysiology, $Ca^{2+}$ imaging and immunohistochemistry) were regulated under the Animals (Scientific Procedures) Act 1986 Amendment Regulations 2012. The University of Cambridge Animal Welfare and Ethical Review Body also approved all animal experiments. Male C57BL/6J mice (Envigo) were housed in groups of up to five per cage with access to food and water *ad libitum*. The

holding room was maintained at 21 °C and operated a 12-hour light/dark cycle. Sensory neurons innervating the site of interest were labeled with the retrograde tracer Fast Blue (2% w/v in sterile PBS; Polysciences) one week before intraplantar injection of carrageenan or one day before intra articular injection of MIA under inhalation anesthesia (2% isoflurane). To label cutaneous hind paw afferents 3 × 1 μl injections were made to the lateral, central and medial plantar aspects of each hind paw, 1.5 μl tracer was injected intra articularly to both knees to label knee-innervating sensory neurons. Unilateral (side determined randomly) injections of carrageenan (20 μl intraplantar; 3% w/v λ-carrageenan in sterile PBS; Sigma-Aldrich) or MIA (10 μl intra articular; 0.1 mg/μl in sterile PBS; Sigma-Aldrich) were made under inhalation anesthesia (2% isoflurane). Digital calipers were used to measure knee, ankle or foot pad diameters at appropriate time points. One cohort of animals were injected with gabapentin (30 mg/kg; Merck) intraperitoneally 10 days post-intra articular injection of MIA.

**Animals (University of Pennsylvania and Columbia University)—**Wild Type male mice of C57BL/6N background were used for behavioral analyses. All mice were adults between 2 and 4 months. Mice for behavior testing were maintained in a barrier animal facility in either the Carolyn Lynch building at the University of Pennsylvania, or the Jerome Greene Science Center at Columbia University. Both vivariums are temperature controlled and maintained under a 12-hr light/dark cycle (7 am/7 pm) at 70 degrees Fahrenheit with ad lib access to food (Purina LabDiet 5001) and tap water. The feed compartment on the wire box lid of the cage was kept at a minimum of 1/3 full at all times. All cages were provided with nestlets to provide enrichment. All procedures were conducted according to animal protocols approved by the university Institutional Animal Care and Use Committee (IACUC) and in accordance with the National Institutes of Health (NIH) guidelines. C57BL6 male mice were purchased from Jackson Laboratories. All animals were habituated to our facility for 2 weeks after delivery before beginning behavioral experiments described below. Animals were co-housed with 4–5 mice per cage in a large holding room containing approximately 500 cages of mice. 20 μl 3% (w/v) λ-Carrageenan (Sigma-Aldrich) in 0.9% sterile NaCl solution (saline) was injected into the mouse hind paw. Mechanical sensitivity was assessed with PAWS at baseline, 4 and 24 hours post carrageenan injection. Inflammation was induced while mice were under inhalation anesthesia (2 to 3.5% isoflurane according to mice's loss of consciousness and anesthetic depth (monitoring of respiratory rate and pattern and responsiveness to toe pinch). Saline or meloxicam (5mg/kg, Henry Schein Animal Health) was injected intraperitoneally 22 hours post carrageenan injection (2 hours before the last PAWS behavioral testing session).

## METHOD DETAILS

**Histology—**Knee joints were collected post-mortem and fixed in 4% (w/v) paraformaldehyde (PFA; Sigma) for 24-hours at 4 °C, tissue was incubated in decalcifying solution (10% (w/v) EDTA, 0.07% (v/v) glycerol, 15% (w/v) sucrose in PBS, pH 8) at 4 °C for ~ 3 weeks, during which time solution was regularly refreshed. Once sufficiently decalcified, joints were snap-frozen in Shandon M-1 Embedding Matrix (Thermo Fisher Scientific). A cryostat was used to slice 20 μm sections in the sagittal plane, sections were collected on SuperFrost Plus slides (Thermo Fisher Scientific). Slides were stained with

safranin O (0.1% w/v, cartilage stain), Weiger"s iron hematoxylin (nuclei stain) and Fast Green (0.08% w/v, counterstain), mounted with glycerol and imaged using a NanoZoomer S360 (Hamamatsu).

**Behavior: Dynamic Weight Bearing—**The weight bearing of free-moving animals was assessed using a dynamic weight bearing apparatus (Bioseb). Each test lasted three minutes, mice were naïve to the test device before baseline weight bearing was assessed. The 2 highest confidence levels of automatic paw assignment by the accompanying software were taken forward for analyses; correct paw assignment was manually validated for at least 1 minute 30 seconds of each test.

**Behavior: Hargreaves Assay—**To assess hind paw heat sensitivity, Hargreaves' test was conducted using a plantar test device (IITC). Mice were placed individually into Plexiglas chambers on an elevated glass platform and allowed to acclimate for at least 30 minutes before testing. A mobile radiant heat source of constant intensity was then applied to the glabrous surface of the paw through the glass plate and the latency to paw withdrawal measured. Paw withdrawal latency is reported as the mean of three measurements for both hind paws with at least a 5 min pause between measurements. A cut-off of 20 s was applied to avoid tissue damage.

**Behavior: Pressure application measurement—**Mechanical sensitivity of the knee joint was assessed using a pressure application measurement device (Ugo Basile). Animals were scruffed before the force transducer was used to apply gradual force to each of the animals' knee joints, by squeezing the joint medially. The withdrawal threshold was recorded when an animal withdrew the limb being tested, or after 450 g force was applied. Each animal was tested twice per time point, with a short break between tests, withdrawal force is reported as an average of the two measurements taken at each time point.

**Electrophysiology—**Mice were sacrificed by cervical dislocation before the lumbar DRG (L2 – L5) from carrageenan injected and non-injected sides were collected separately in dissociation media (L-15 + GlutaMAX growth media supplemented with 24 mM $NaHCO_3$; Life Technologies). Dissected DRG were then incubated in dissociation media containing 1 mg/ml type 1A collagenase (Sigma Aldrich) and 6 mg/ml bovine serum albumin (BSA; Sigma-Aldrich) for 15 min at 37 °C, 5% $CO_2$, before a further 30 min in dissociation media containing 1 mg/ml trypsin (Sigma-Aldrich) and 6 mg/ml BSA. DRG were then suspended in culture media (L-15 + GlutaMAX growth media supplemented with 10% (v/v) fetal bovine serum, 24 mM $NaHCO_3$ 38 mM glucose and 2% (v/v) penicillin/streptomycin) before several rounds of mechanical trituration and brief centrifugation (160g, 30 s). After sufficient trituration, dissociated cells were pelleted (160g, 5 min), resuspended in culture media and plated on poly-D-lysine/laminin coated glass coverslips (BD Biosciences) and incubated at 37 °C, 5% $CO_2$. Electrophysiology experiments were performed the following day, recordings were made using an EPC-10 amplifier (HEKA) and corresponding Patchmaster software. The extracellular solution contained (in mM): NaCl (140), KCl (4), $MgCl_2$ (1), $CaCl_2$ (2), glucose (4) and HEPES (10), adjusted to pH 7.40 with NaOH. Patch pipettes were pulled from borosilicate glass capillaries (Hilgenberg) using a P-97 pipette

puller (Sutter Instruments) with resistances of 4–8 MΩ and back filled with intracellular solution containing (in mM): KCl (110), NaCl (10), $MgCl_2$ (1), EGTA (1), HEPES (10), $Na_2ATP$ (2), $Na_2GTP$ (0.5), adjusted to pH 7.30 with KOH. Whole cell currents or voltages were sampled at 20 kHz from Fast Blue labelled neurons, identified by LED excitation at 365 nm (Cairn Research). Step wise depolarization (Δ10 pA, 50 ms) was used to determine the action potential threshold of cells. Only cells which fired action potentials and had a resting membrane potential less than or equal to −40 mV and were included in analyses. Action potential parameters were measured using Fitmaster software (HEKA) and IgorPro software (Wavemetrics) as previously described[18]. The excitability of neurons was further assessed by applying a suprathreshold (2x action potential threshold) for 500 ms, the number of action potentials discharged during this time was counted. The activity of macroscopic voltage-sensitive channels was assessed in voltage clamp mode with appropriate compensation for series resistance. Cells were held at −120 mV for 150 ms before stepping to the test potential (−60 mV – 55 mV in 5 mV increments) for 40 ms and returning to a holding potential of −60 mV for 200 ms between steps. Peak inward and outward currents were normalized to cell size by dividing by cell capacitance. Peak inward current densities were then fit to a Boltzmann function to determine the reversal potential and half-activating potential of voltage sensitive channels. To compare macroscopic voltage-sensitive currents between neurons isolated from the Ipsi and Contra sides peak current densities were normalized to those obtained from cells from the Contra side.

**$Ca^{2+}$ Imaging—**During the dissociation and culture of DRG neurons isolated from mice that were injected with MIA intra articularly one coverslip was seeded at double the density for electrophysiology experiments for both ipsilateral and contralateral cells. 24-hours after dissociation these cells were incubated with the $Ca^{2+}$ indicator Fluo-4 AM (10 μM diluted in the same extracellular solution used for electrophysiology experiments) for 30 minutes at 37 °C, 5% $CO_2$. Following the 30 minute incubation, coverslips were washed and imaged using an inverted Nikon Eclipse T*i* microscope, Fluo-4 was excited using a 470 nm LED (Cairn Research) and captured with a Zyla cSMOS camera (Andor) at 1 Hz, 50 ms exposure using Micro-Manager software (NIH). Cells were perfused via a gravity-driven 12-barrel perfusion system (Dittel). A 15 second baseline was captured while extracellular solution was perfused before a 10 second stimulation with 1 μM capsaicin (Sigma-Aldrich), cells were then perfused with extracellular solution again for 75 seconds before challenge with 50 mM KCl, sufficient to depolarize and thus identify viable neurons. After each experiment a single image was captured at 365 nm (Cairn Research), exposure 500 ms, to identify Fast Blue positive cells. During analysis, single cells were selected as regions of interest using ImageJ software (NIH). Cells were deemed positive for Fast Blue if the background corrected intensity exceeded 2x the standard deviation (SD) of intensities of all cells in the field of view). $Ca^{2+}$ signals were analyzed with custom-written R scripts, the fluorescence signals of each cell were background and baseline corrected, only cells for which KCl elicited an increase in Fluo-4 fluorescence > 5 x the SD of the baseline average were taken forward for further analyses. Fluo-4 intensities were normalized to the maximal fluorescence elicited during KCl stimulation, cells were deemed capsaicin sensitive if Fluo-4 intensity surpassed the same threshold during the 10 second application of capsaicin.

**Immunohistochemistry—**24-hours post inflammation a cohort of mice were transcardially perfused with 4% (w/v) PFA under terminal anesthesia (intraperitoneal delivery of 200 mg/kg sodium pentobarbital). Lumbar DRG (L3 – L4) were then collected from both the inflamed and non-injected sides and post-fixed in Zamboni's fixative for 30 min, followed by overnight incubation in 30% (w/v) sucrose at 4 °C for cryoprotection. Individual DRG were then snap-frozen in Shandon M-1 Embedding Matrix (Thermo Fisher Scientific). 12 μm sections of each DRG were collected on a cryostat sequentially across 10 slides. After washing with PBS containing 0.001% (v/v) Tween-20 (Thermo Fisher Scientific), slides were incubated with antibody diluent (1 % (w/v) BSA, 5% (v/v) donkey serum and 0.02% (v/v) Triton-X-100 in PBS) at room temperature for 1 hour before overnight incubation at 4 °C with an anti-TRPV1 antibody (1:500; guinea-pig polyclonal; Alomone, AGP-118). The following day slides were washed three times with PBS-Tween before incubation with donkey anti guinea-pig IgG-AF488 for 2 hours at room temperature, followed by a further two washes and mounting. Images were acquired with an Olympus BX51 microscope and Q-Imaging camera. Two sections per DRG per animal were analyzed, briefly, each cell was selected as a region of interest and individual cells were considered positively stained if the background corrected intensity exceeded 2x SD of the normalized intensity across all sections. Negative controls which were not exposed to any primary antibody showed no fluorescent staining.

**High-speed imaging and video storage—**Mouse behaviors were recorded at 2000 fps with a high-speed camera (Photron FastCAM Mini AX 50 170 K-M-32GB- Monochrome 170K with 32 GB memory) and attached lens (Zeiss 2/100M ZF.2- mount). Mice performed behavior in rectangular plexiglass chambers on an elevated mesh platform. The camera was placed at a ~45° angle at ~1–2 feet away from the Plexiglas holding chambers on a tripod with geared head for Photron AX 50. CMVision IP65 infrared lights that mice cannot detect were used to adequately illuminate the paw for subsequent tracking in ProAnalyst. All data were collected on a Dell laptop computer with Photron FastCAM Analysis software (average size of video file = ~2 GB).

**Somatosensory behavior assays—**In all behavioral experiments, we used a sample size of 6–10 mice per strain, as these numbers are consistent with studies of this kind in the literature to reach statistically significant conclusions. All mice were habituated for 2 days, for one hour each day, in the Plexiglas holding chambers before testing commenced. Mice were tested in groups of five and chambers were placed in a row with barriers preventing mice from seeing each other. On testing day, mice were habituated for an additional ~10 min before stimulation and tested one at a time. Stimuli were applied through the mesh to the hind paw proximal to the camera. Testing only occurred when the camera's view of the paw was unobstructed. Mice received two stimuli on a given testing day (db and lp) and were given at least 24 hr between each stimulus session. Stimuli were tested from least painful to most: dynamic brush then light pinprick. Dynamic brush tests were performed by wiping a concealer makeup brush (L'Oréal Paris Infallible Concealer Brush, item model number 3760228170158) across the hind paw from back to front. Light pinprick tests were performed by touching a pin (Austerlitz Insect Pins) to the hind paw of the mouse. The pin was withdrawn as soon as contact was observed.

**Automated paw tracking (Proanalyst)—**We used ProAnalyst software to automatically track hind paw movements following stimulus application. This software allowed us to integrate automated and manually scored data, possible through the 'interpolation' feature within ProAnalyst. We were able to define specific regions of interest (paw), track, and generate data containing 'x' and 'y' coordinates of the paw through time. In a subset of videos, additional manual annotation was performed for increased accuracy.

**Automated paw tracking (DeepLabCut)—**For deep learning-based paw tracking in DeepLabCut (DLC), we pseudo-randomly selected a subset of training frames from trials which contained the greatest behavioral variation and hand-labeled the hind paw toes, center, and heel. We trained DLC to predict toe, center, and heel positions in unlabeled video frames.

**Quantifying withdrawal behavior (PAWS)—**Behavioral features were extracted from raw paw position time series in an automated and standardized procedure. First, the start and end of paw movement (paw at rest on the ground) were identified, and analysis was restricted to this time window. Peaks in paw height were then determined based on Savitsky-Golay smoothed estimates of paw velocity, and the first peak identified. The time of the first peak (designated t*) was used to separate pre-peak behavioral feature calculations from post-peak calculations. To differentiate shaking from guarding in the post-peak period, we constructed a moving reference frame based on the principal axis of paw displacement across a sliding window (0.04 s in duration) for each time point, and identified periods of consecutive displacements above a specified threshold (35% of maximum paw height) as periods of shaking. Note that in the construction of the moving reference frame the principal axes of variation were recovered via principal component analyses, which is not invariant to the sign of the recovered axes. Since displacement is measured over time it is sensitive to reversals in sign along the axis we measure it. We therefore ensured consistency by using the axis direction minimizing the angular deviation from the axis recovered at the previous time step. PAWS is open source and freely available at https://github.com/crtwomey/paws.

**Quantifying withdrawal behavior (B-SOiD)—**To determine behavioral sub-actions following foot stimulation, pose estimation data was passed along to the unsupervised behavioral discovery and extraction algorithm, B-SOiD. Experimentalists processing this data were blind to the experimental condition. Position coordinates of fore paw hind paw motion tracked by DeepLabCut in samples of 2000fps video, and then were imported to the B-SOiD app to identify unique behavioral clusters in response to pain stimulus. Data from dynamic brush and light prick Hour-4 sessions were combined to develop a generalized B-SOiD model of pain response. The frame rate was scaled down to $1/^{7}$th of the original to help B-SOiD extract sub behavioral features. Data used in the B-SOiD model were the hind paw toe, hind paw center-paw and two static reference positions. The two static reference points were the initial positions of the fore paw the maximum elevation of toe post stimulation. B-SOiD performed nonlinear embedding to transform 16-dimensional data to 5- dimensional UMAP space. The 16-dimensional data include frame by frame calculation of distance and angle between all four points as well as the speed of the two body parts. 11 behavioral clusters were identified and used to train the random forest classifier of the

algorithm, which was then used to assign behavioral labels to data from all epochs and stimulation types. Every frame was labeled, and a smoothing kernel was used to eliminate any sub actions lasting under 2.5 seconds (5 frames). Importantly, beyond the spatiotemporal relationship values between the points, no other information was available to the algorithm. B-SOiD is open source and freely available at https://github.com/YttriLab/B-SOID.

**3D pose analysis: data acquisition, processing, and modeling—**Analysis was performed using tools and procedures provided by the Datta Lab, and following previous publications[24–26]. The following programs and versions were used: kinect2-nidaq (v0.2.4-alpha), moseq2-extract (v1.1.2), moseq2-pca (v1.1.3), moseq2-model (v1.1.2), moseq2-viz (v1.2.0). All depth movie data for this study were used together to train the final MoSeq model: carrageenan cohort, saline control cohort, MIA cohort.

First, we used the program kinect2-nidaq (v0.2.4-alpha) to collect raw depth frames from a Microsoft Kinect, mounted above the arena. Frames were collected at 30 Hz, and each frame was composed of 512 × 424 pixels, where each pixel contained a 16-bit unsigned integer specifying the distance of that pixel from the sensor in mm. After each session, frames were gzip compressed and moved to another computer for offline analysis.

The raw data for each recording session was extracted using the program moseq2-extract (v1.1.2), largely using the default parameters and the flip model “flip_classifier_k2_c57_10to13weeks.pkl” supplied by the Datta Lab. Briefly, the mouse’s center and orientation were found using an ellipse fit on the pixels identified as “mouse”. Then, an 80 × 80 pixel box was drawn around the mouse, and the mouse was rotated to face the right hand side. All extraction results were assessed for quality of extraction by a human watching a movie visualization of the data and also by comparing the distributions of height, width, length, and area, following best practices as described by the Datta Lab (personal communication).

Next, we used the program moseq2-pca (v1.1.3) to project the extracted depth frames onto the first 10 learned principal components (PCs), forming a 10 dimensional time series that described the mouse’s 3D pose trajectory. Quality of the PCA model was assessed by examining a visualization of the pixel weights assigned by each principal component as well as the cumulative distribution of the percent variance explained by each principal component. This program was also used to generate a model-free changepoint analysis, which describes an empirical module duration distribution, found without any model constraints.

Then we used the program moseq2-model (v1.1.2) and the 10-D PCA-transformed data to train a series of autoregressive hidden Markov models (AR-HMM, a.k.a “MoSeq model”). Each state was described by a vector autoregressive process that captures the evolution of the 10 PCs over time and a hidden Markov model that captures the switching dynamics between these states. For all models, we used the following parameters: “--max-states 100 --robust”. We determined the best value for the hyperparameter kappa, which affects the timescale of discovered behavioral modules. For this we trained a family of 100 models for 200 iterations each, with kappa values ranging logarithmically from 100,000 to 1,000,000,000. The best

kappa parameter was determined by minimizing the absolute difference in the mean module duration between a given AR-HMM model fit and the mean block duration found via a model-free changepoint analysis (see above). For the results presented in this manuscript, we found a kappa value of 155,567,614 satisfied this criteria. Then, we trained a family of 100 models for 1,000 iterations each, using this discovered optimal kappa value. To choose an appropriate model from this family, we examined the aggregate log-likelihood value for each model and chose the model with the median log-likelihood to carry forward to downstream analysis.

**3D pose analysis: Behavioral usage and transition matrix analysis—**Module usage was calculated by counting the number of occurrences of each module and dividing by the total sum of all module occurrences within a recording session, converting module usage into a percentage. The number of modules analyzed were cutoff based on the global usage across all sessions, eliminating modules which were not performed by any animals in the study. Transition matrices were calculated by counting the total number of occurrences where module A transitions into module B (for all modules) and normalizing by the sum of the matrix (bigram normalization). Statistical testing for module usage follows the previously published procedures[24–26,96]. Briefly, for each group comparison of interest and each module, we took 1,000 bootstrap samples (sampling with replacement within a group) of the given module's usage for each group and performed a z-test on these two distributions. Finally, we use the Benjamini-Hochberg procedure (statsmodels.stats.multitest.multipletests[97]) to correct for multiple hypothesis testing and control the false discovery rate.

**3D pose analysis: Behavioral Linear Discriminant Analysis—**Linear Discriminant Analysis (LDA) was performed using the scikit-learn implementation using the eigen solver and 2 components. Individual normalized usage or bigram transition probabilities were fed as input to the LDA model, including group labels. This data was split into train and validation sets in a 70:30 stratified ratio. We searched over the hyperparameter "shrinkage" using a 5-fold stratified cross-validation approach using only the train subset and found little effect on the model performance against the never-before-seen validation set. Final models were trained using the entire train set, and evaluated on the never-before-seen validation set. We also performed a permutation test (sklearn.model_selection.permutation_test_score), wherein we train a family of models against 100 randomly permuted labels, and compare the distribution of model scores against shuffled data vs final model and calculate a p-value. Results were plotted with seaborn and matplotlib.

**Learned Embeddings of module Sequences—**Each animal was represented as a doc2vec ("document to vector") embedding[98] using the Gensim software package (Software Framework for Topic Modelling with Large Corpora. In Proceedings of LREC 2010 workshop New Challenges for NLP Frameworks. Valletta, Malta: University of Malta, 2010. p. 46--50. ISBN 2-9517408-6-7), version 4.0.1, in Python 3. Doc2vec is a standard unsupervised sequence embedding technique used widely in natural language processing. Each animal and each module was first encoded uniquely as a one-hot vector of $d$ dimensions (d = 148 = 78 animals + 70 modules in the MIA condition or d = 130 = 60

animals + 70 modules in the Carrageenan condition). These one-hot vectors were mapped by a linear transformation to an $n$-dimensional embedding space. The linear transformation was adapted by stochastic gradient descent using two losses, resulting in two embeddings. Following Le and Mikolov, 2014, the two embeddings for each animal were averaged to produce the final animal representation. Both embeddings were trained with standard procedures which we outline here. The first embedding was learned by 1) randomly sampling an animal and a contiguous length-$2k$ sequence of modules emitted by the animal, 2) mapping the one hot vectors of the sampled animal and modules to the $n$-dimensional embedding space, 3) averaging the animal and module embeddings, 4) mapping the average to the 70-dimensional space of probability distributions over modules, and 5) predicting from this output the identity of a random module in the size-$2k$ window. The embedding space was adapted to improve accuracy on this module prediction task. In the parlance of doc2vec methods, this is "distributed memory" (DM) embedding. The second embedding was learned using only representations of animals (no module embeddings). Similar to the first technique, an animal was randomly sampled together with a $2k$-module subsequence in its raw behavioral sequence. The one hot vector of only the animal was mapped to the embedding space. The animal embedding was then mapped to the $2k$ x 70 dimensional space of distributions on $2k$-long module subsequences, from which random modules in the sampled subsequence window were predicted. The embedding space was adapted to improve the accuracy of this subsequence prediction task, which also helps the embedding encode higher order information beyond neighboring modules in the raw sequence. This is referred to as a "distributed bag of words" (DBOW) embedding. Again, the final embedding for each animal to be used in classification was the concatenation of DM and DBOW embeddings. In order to determine the best possible embedding model, we performed a hyperparameter grid search over the embedding dimension, ($n$, between 10 and 100 in 10 equally-spaced steps), the embedding window size, ($k$ = 2, 4, 8, 16, 32), the number of training epochs, ($e$=50, 100, 150, 200, 250) and the type of raw data used. For raw data, we either used the modules assigned to every video frame ("frames" data), or the discrete sequence of modules independent of their real-time duration ("emissions" data). The search revealed that the model with the best training accuracy (see below) had $n$ = 70 $k$=2, $e$=50 and used the emissions data. Note that, although the identity of an individual animal was used during training, the embeddings are not trained to distinguish between different animals. Moreover, the experimental class of each animal was never used at this stage.

**Classifier Analysis of Animal Representations—**We used a multinomial logistic regression classifier to compare the expressive power of three types of animal representations: module usages, module transition probabilities, and learned embeddings. Our goal here was to predict which of the five experimental manipulations an animal received from each of these representations. The dimensionality of the input data was generally different in the three cases, with usages fixed at 70 dimensions. For transitions, we used the $m$ most frequent transitions on average, where $m$ was chosen by a grid search having the same values as the $n$ search discussed above (m=50 was optimal). Data in each representation condition was first separated into the same train and test sets in a 70–30 split. We trained an identical, L2 -regularized, 5-class logistic regression classifier on each type of representation using leave-one-out cross validation on the training set. The regularizer

weight was chosen by a grid search over 11 values logarithmically spaced between 1 × 10–5 and 1 × 105 and all results represent the best regularization weight for each model. The classifier was trained using scikit-learn in Python 3. The classifier was trained with a stopping criterion of 1 × 10–5 and with balanced class correction in a one-vs-rest manner. For each representation type, we chose (over different grid search parameters; see previous section) the model which had the best accuracy on the training set. We then report the F1 score for this model on the testing set; i.e. hyperparameters were not tuned according to the reported F1 score, only the training F1 score. In the MIA condition, this procedure resulted in the following testing F1 scores per representation: (Usages, .481 ± .240), (Transitions, .410 ± .160), (Embeddings, .781 ± .190). In the carrageenan condition: (Usages, .223 ± .190), (Transitions, .257 ± .164), (Embeddings, .194). Standard errors are reported. Since the embeddings take into account much larger scale information (i.e. windows of 2k = 4 modules), we can hypothesize consequently that there are experimental effects which differentiate the groups and manifest at behavioral scales beyond usages and one-step transitions.

**Finding characteristic module sequences—**There are several possible ways to associate to each embedding a set of characteristic modules or module sequences. For the present study, we adapted a standard method (Mikolov et al., 2013) for scoring the significance of *n*-grams in written text. An *n*-gram is a contiguous sequence of *n* words or, in our case, modules. The original method scored the significance of a bigram *(w1, w2)* by computing

$$s'(w1, w2) = (C(w1, w2) - \delta)/((w1) . C(w2))$$

where *C(x)* represents the counts of x in the data and δ controls how many counts are required to make s positive. The idea is to discount the significance of the bigram *(w1, w2)* by the amount that *w1* and *w2* tend to appear individually (including in the bigram of interest). The original authors detected higher order n-grams by applying this scoring function to sequences repeatedly, thresholding *s* to determine which bigrams should become a fixed phrase, and congealing detected phrases into single symbols.

We took a similar approach with a new emphasis on module n-grams which distinguished between animal classes. To that end, let *A* be the module sequences associated to a given experimental class (e.g. baseline), and -*A* be the complementary module sequences of all other animals in all other classes. Further, for a given *n*-gram *w = (w1, …, wn)*, denote the set of contiguous subgrams of lengths 1, …, *n* by S(*w*) = {(*w1*), (*w2*), …,(*w1,w2*, …), (*w2, w3*), …}. Then, we define

$$s'(w) = (C_A(w) - \delta)/\pi S(w) C - A(w)$$

In other words, we discount the n-grams detected in class A by the amount that all subgrams, including the n-gram itself, appear in -A. If any subgram was found in A but not in the complement, we gave it a count of ε = 1 × 10–3. δ was set to 1. We collected scores for 2,3 and 4 grams and then found the unique n-grams associated to each class. We

also experimented with setting the complement (i.e. -A) as the whole data set (including A), but this produced worse quantitative results than Eq. S.2. We took to the top 5% of detected phrases by score per class.

The scoring function which we used to identify significant phrases is an adaptation of standard methods used in natural language processing (see òriginal scorer`[99]). By construction, this function discounts the score of a detected phrase to the extent that its constituent modules appear individually due to random chance. Take, for example, the top detected phrases for the 4-hour class in the CAR condition, “65>62”. Module 65 appears 8 times, each time it appears it does so followed by Module 62, Module 62 appears 13 times. The scorer detected this regularity and awards “65>62” the highest rank (5.3846). Compare this to the case of “0>1”, where each syllable appears many thousands of times individually (Module 0: 1046 times; Module 1: 1306 times), but the intact bigram appears only 4 times. The resulting score (0.0002) is therefore 27000 times smaller than that of “65>62”. Our modified version of this score function, described in the section “Finding characteristic module sequences”, further exaggerates these scores by additionally discounting them by the amount the intact phrase appears outside of the target class (e.g., in this case not in 4-hour CAR).

Put simply, the above analysis shows that certain phrases (e,g. 65>62) tend to appear only as intact units rather than accidental neighbors. We show this by counting the number of times that 62 immediately follows 65 and dividing by the total count of 65 or 62 in the whole sequence of behaviors. If the phrase 65>62 appeared frequently only because 65 and 62 appeared on their own many times (due to random chance), then this division would lower the score, exactly like the case of 0>1. A high score indicates that the phrase appears not due to random chance but because those modules, in some sense, belong together.

To show that these n-grams have a material effect on the quality of the learned embeddings, we then ablated them and replaced them with random modules in the raw data. The number of ablations was proportionally small (MIA: 3 days 1.15%, Baseline + saline 0.15%, 10-days + gaba 0.22%, 10 days + saline 0.11%, Baseline + gaba .08%. Carrageenan: 4-hours .98%, Baseline + meloxicam .03%, Baseline + saline .13%, 24-hours + meloxicam 2.1%, 24-hours + saline .15%) of the raw modules. Averaging over ten realizations of random module insertions, F1 dropped, in the MIA condition, from .781 to .620 +/− .011 (s.e.), and, in the carrageenan condition, from .538 to .301 +/− .075. Since the optimal window size was 2k = 4, performance would likely have degraded even more had we ablated higher order n-grams, though these are difficult to find. To show that targeting these specific phrases was the cause of the decrease in classifier performance, we also ablated random phrases, making sure to ablate the same amount as in the targeted condition. However, in this case we found that testing F1 decreased only by .015 in the MIA condition and increased very slightly by .002 in the carrageenan condition The top ranked n-grams for each class for each condition are given in Tables S2 and S3.

## QUANTIFICATION AND STATISTICAL ANALYSIS

Data are presented as the mean ± standard error of the mean (SEM). Statistical tests used to assess differences between groups are detailed in individual figure legends. Behavioral

assays were replicated several times (3 to 10 times depending on the experiments) and averaged per animal, except for PAWS where each stimulus was presented one time to each animal per type of stimulus (brush or pinprick) during the testing session to avoid sensitization. Statistics were then performed over the mean of animals. Statistical analysis was performed in GraphPad Prism (USA) using two-sided paired or unpaired Student's t-tests, one- or two-way repeated-measures ANOVA for functional assessments, when data were distributed normally. Post hoc Tukey's or Bonferroni tests were applied when appropriate. The significance level was set as $p < 0.05$. The nonparametric Mann-Whitney or Wilcoxon signed rank tests were used in comparisons of <5 mice.

## Supplementary Material

Refer to Web version on PubMed Central for supplementary material.

## Acknowledgements

We thank Sherry Lin and members of the Datta lab for valuable discussions. LAP and EStJS acknowledge the work of University of Cambridge Combined Animal Facility staff. LAP was supported by the University of Cambridge BBSRC Doctoral Training Programme (BB/M011194/1). HH was funded by a BBSRC/GSK iCASE PhD studentship (BB/V509528/1). EStJS acknowledges support from Versus Arthritis (RG 21973) and the MRC (MR/W002426/1). IAS and lab members acknowledge support from start-up funds provided by the University of Pennsylvania and Columbia University, National Institute of Health grants K99/R00 and DP2 New Innovator, and fellowships from the Rita Allen Foundation, Pew Charitable Trust, Brain Research Foundation and Alfred P. Sloan Foundation. EAY is supported by the NIH (R01NS110483, R01DA053014). VEA, MAT, MB are supported by startup funds from Rutgers University. VEA and MB are also supported by the Pew Charitable Trust, the New Jersey Commission on Spinal Cord Research (CSCR20IRG005) and the NIH (NIH/NINDS R01NS124799; NIH/NINDS R01NS119268; NIH/NINDS K01NS116224). MAT is also supported by Tourette Association of America, New Jersey Center for Tourette Syndrome, and a Robert Wood Johnson foundation grant.

## Inclusion and Diversity Statement

All the authors in this study actively support inclusion, diversity, and equality in science. The two senior authors, and several co-authors are from racial and ethnic groups underrepresented in science. Gender and sexual orientation diversity is also highlighted in the composition of this team, including representation of women as the first and last author. One or more of the authors of this paper received support from a program designed to increase minority representation in science, including the PDEP fellowship from Burroughs Wellcome Fund. While citing references scientifically relevant for this work, we also actively worked to promote gender balance in our reference list.

## References

1. Smith ESJ, and Lewin GR (2009). Nociceptors: a phylogenetic view. J. Comp. Physiol. A Neuroethol. Sens. Neural Behav. Physiol 195, 1089–1106. [PubMed: 19830434]
2. Walters ET, Crook RJ, Neely GG, Price TJ, and Smith ESJ (2023). Persistent nociceptor hyperactivity as a painful evolutionary adaptation. Trends Neurosci. 46, 211–227. [PubMed: 36610893]
3. Ghouri A, and Conaghan PG (2019). Treating osteoarthritis pain: recent approaches using pharmacological therapies. Clin. Exp. Rheumatol 37 Suppl 120, 124–129. [PubMed: 31621576]
4. Ghouri A, and Conaghan PG (2019). Update on novel pharmacological therapies for osteoarthritis. Ther. Adv. Musculoskelet. Dis 11, 1759720X19864492.

5. da Costa BR, Pereira TV, Saadat P, Rudnicki M, Iskander SM, Bodmer NS, Bobos P, Gao L, Kiyomoto HD, Montezuma T, et al. (2021). Effectiveness and safety of non-steroidal anti-inflammatory drugs and opioid treatment for knee and hip osteoarthritis: network meta-analysis. BMJ 375, n2321. [PubMed: 34642179]
6. Xu GY, and Zhao ZQ (2001). Change in excitability and phenotype of substance P and its receptor in cat Abeta sensory neurons following peripheral inflammation. Brain Res. 923, 112–119. [PubMed: 11743978]
7. Tanaka M, Cummins TR, Ishikawa K, Dib-Hajj SD, Black JA, and Waxman SG (1998). SNS Na+ channel expression increases in dorsal root ganglion neurons in the carrageenan inflammatory pain model. Neuroreport 9, 967–972. [PubMed: 9601651]
8. Morris CJ (2003). Carrageenan-induced paw edema in the rat and mouse. Methods Mol. Biol 225, 115–121. [PubMed: 12769480]
9. Hargreaves K, Dubner R, Brown F, Flores C, and Joris J (1988). A new and sensitive method for measuring thermal nociception in cutaneous hyperalgesia. Pain 32, 77–88. [PubMed: 3340425]
10. Buisseret B, Guillemot-Legris O, Muccioli GG, and Alhouayek M (2019). Prostaglandin D-glycerol ester decreases carrageenan-induced inflammation and hyperalgesia in mice. Biochim. Biophys. Acta Mol. Cell Biol. Lipids 1864, 609–618. [PubMed: 30684679]
11. Pitcher T, Sousa-Valente J, and Malcangio M (2016). The Monoiodoacetate Model of Osteoarthritis Pain in the Mouse. J. Vis. Exp 10.3791/53746.
12. Murphy SL, Lyden AK, Kratz AL, Fritz H, Williams DA, Clauw DJ, Gammaitoni AR, and Phillips K (2015). Characterizing Pain Flares From the Perspective of Individuals With Symptomatic Knee Osteoarthritis. Arthritis Care Res. 67, 1103–1111.
13. Stevenson GW, Mercer H, Cormier J, Dunbar C, Benoit L, Adams C, Jezierski J, Luginbuhl A, and Bilsky EJ (2011). Monosodium iodoacetate-induced osteoarthritis produces pain-depressed wheel running in rats: implications for preclinical behavioral assessment of chronic pain. Pharmacol. Biochem. Behav 98, 35–42. [PubMed: 21147151]
14. Burston JJ, Mapp PI, Sarmad S, Barrett DA, Niphakis MJ, Cravatt BF, Walsh DA, and Chapman V (2016). Robust anti-nociceptive effects of monoacylglycerol lipase inhibition in a model of osteoarthritis pain. Br. J. Pharmacol 173, 3134–3144. [PubMed: 27501482]
15. Miyake S, Higuchi H, Honda-Wakasugi Y, Fujimoto M, Kawai H, Nagatsuka H, Maeda S, and Miyawaki T (2019). Locally injected ivabradine inhibits carrageenan-induced pain and inflammatory responses via hyperpolarization-activated cyclic nucleotide-gated (HCN) channels. PLoS One 14, e0217209. [PubMed: 31125368]
16. Sun J, Song F-H, Wu J-Y, Zhang L-Q, Li D-Y, Gao S-J, Liu D-Q, Zhou Y-Q, and Mei W (2022). Sestrin2 overexpression attenuates osteoarthritis pain via induction of AMPK/PGC-1α-mediated mitochondrial biogenesis and suppression of neuroinflammation. Brain Behav. Immun 102, 53–70. [PubMed: 35151829]
17. Davidson S, Copits BA, Zhang J, Page G, Ghetti A, and Gereau RW 4th (2014). Human sensory neurons: Membrane properties and sensitization by inflammatory mediators. Pain 155, 1861–1870. [PubMed: 24973718]
18. Chakrabarti S, Pattison LA, Singhal K, Hockley JRF, Callejo G, and St. John Smith E Acute inflammation sensitizes knee-innervating sensory neurons and decreases mouse digging behavior in a TRPV1-dependent manner. 10.1101/350637.
19. Mao J (2012). Current challenges in translational pain research. Trends in Pharmacological Sciences 33, 568–573. 10.1016/j.tips.2012.08.001. [PubMed: 22959652]
20. Sadler KE, Mogil JS, and Stucky CL (2022). Innovations and advances in modelling and measuring pain in animals. Nat. Rev. Neurosci 23, 70–85. [PubMed: 34837072]
21. Jones JM, Foster W, Twomey CR, Burdge J, Ahmed OM, Pereira TD, Wojick JA, Corder G, Plotkin JB, and Abdus-Saboor I (2020). A machine-vision approach for automated pain measurement at millisecond timescales. Elife 9. 10.7554/eLife.57258.
22. Mathis A, Mamidanna P, Cury KM, Abe T, Murthy VN, Mathis MW, and Bethge M (2018). DeepLabCut: markerless pose estimation of user-defined body parts with deep learning. Nat. Neurosci 21, 1281–1289. [PubMed: 30127430]

23. Hsu AI, and Yttri EA (2021). B-SOiD, an open-source unsupervised algorithm for identification and fast prediction of behaviors. Nat. Commun 12, 5188. [PubMed: 34465784]
24. Wiltschko AB, Tsukahara T, Zeine A, Anyoha R, Gillis WF, Markowitz JE, Peterson RE, Katon J, Johnson MJ, and Datta SR (2020). Revealing the structure of pharmacobehavioral space through motion sequencing. Nat. Neurosci 23, 1433–1443. [PubMed: 32958923]
25. Markowitz JE, Gillis WF, Beron CC, Neufeld SQ, Robertson K, Bhagat ND, Peterson RE, Peterson E, Hyun M, Linderman SW, et al. (2018). The Striatum Organizes 3D Behavior via Moment-to-Moment Action Selection. Cell 174, 44–58.e17. [PubMed: 29779950]
26. Wiltschko AB, Johnson MJ, Iurilli G, Peterson RE, Katon JM, Pashkovski SL, Abraira VE, Adams RP, and Datta SR (2015). Mapping Sub-Second Structure in Mouse Behavior. Neuron 88, 1121–1135. [PubMed: 26687221]
27. Basbaum AI, Bautista DM, Scherrer G, and Julius D (2009). Cellular and molecular mechanisms of pain. Cell 139, 267–284. [PubMed: 19837031]
28. Latremoliere A, and Woolf CJ (2010). Synaptic plasticity and central sensitization: author reply. J. Pain 11, 801–803. [PubMed: 20674851]
29. Sandkühler J (2010). Central sensitization versus synaptic long-term potentiation (LTP): a critical comment. J. Pain 11, 798–800. [PubMed: 20674850]
30. Weyer AD, Zappia KJ, Garrison SR, O'Hara CL, Dodge AK, and Stucky CL (2016). Nociceptor Sensitization Depends on Age and Pain Chronicity(1,2,3). eNeuro 3. 10.1523/ENEURO.0115-15.2015.
31. Levy L (1969). Carrageenan paw edema in the mouse. Life Sci. 8, 601–606.
32. Fang J, Wang S, Zhou J, Shao X, Sun H, Liang Y, He X, Jiang Y, Liu B, Jin X, et al. (2021). Electroacupuncture Regulates Pain Transition Through Inhibiting PKCε and TRPV1 Expression in Dorsal Root Ganglion. Front. Neurosci 15, 685715. [PubMed: 34354561]
33. Henriques MG, Silva PM, Martins MA, Flores CA, Cunha FQ, Assreuy-Filho J, and Cordeiro RS (1987). Mouse paw edema. A new model for inflammation? Braz. J. Med. Biol. Res 20, 243–249. [PubMed: 3690058]
34. Huang J, Zhang X, and McNaughton PA (2006). Inflammatory pain: the cellular basis of heat hyperalgesia. Curr. Neuropharmacol 4, 197–206. [PubMed: 18615146]
35. Chakrabarti S, Pattison LA, Doleschall B, Rickman RH, Blake H, Callejo G, Heppenstall PA, and St. John Smith E (2020). Intraarticular Adeno-Associated Virus Serotype AAV-PHP.S–Mediated Chemogenetic Targeting of Knee-Innervating Dorsal Root Ganglion Neurons Alleviates Inflammatory Pain in Mice. Arthritis & Rheumatology 72, 1749–1758. 10.1002/art.41314. [PubMed: 32418284]
36. Guay J, Bateman K, Gordon R, Mancini J, and Riendeau D (2004). Carrageenan-induced paw edema in rat elicits a predominant prostaglandin E2 (PGE2) response in the central nervous system associated with the induction of microsomal PGE2 synthase-1. J. Biol. Chem 279, 24866–24872. [PubMed: 15044444]
37. Logashina YA, Palikova YA, Palikov VA, Kazakov VA, Smolskaya SV, Dyachenko IA, Tarasova NV, and Andreev YA (2021). Anti-Inflammatory and Analgesic Effects of TRPV1 Polypeptide Modulator APHC3 in Models of Osteo- and Rheumatoid Arthritis. Mar. Drugs 19. 10.3390/md19010039.
38. Cao E, Cordero-Morales JF, Liu B, Qin F, and Julius D (2013). TRPV1 channels are intrinsically heat sensitive and negatively regulated by phosphoinositide lipids. Neuron 77, 667–679. [PubMed: 23439120]
39. Cao E, Liao M, Cheng Y, and Julius D (2013). TRPV1 structures in distinct conformations reveal activation mechanisms. Nature 504, 113–118. [PubMed: 24305161]
40. Julius D (2013). TRP channels and pain. Annu. Rev. Cell Dev. Biol 29, 355–384. [PubMed: 24099085]
41. Burdge J, Fried NT, and Abdus-Saboor I (2021). Using high-speed videography for objective and reproducible pain measurement on a mouse pain scale. STAR Protoc 2, 100322. [PubMed: 33598658]

42. Liljencrantz J, and Olausson H (2014). Tactile C fibers and their contributions to pleasant sensations and to tactile allodynia. Frontiers in Behavioral Neuroscience 8. 10.3389/fnbeh.2014.00037.
43. Liljencrantz J, Marshall A, Ackerley R, and Olausson H (2014). Discriminative and affective touch in human experimental tactile allodynia. Neuroscience Letters 563, 75–79. 10.1016/j.neulet.2014.01.041. [PubMed: 24486839]
44. Liljencrantz J, Pitcher M, Catherine Bushnell M, and Olausson H (2016). Pain and Touch: Roles for C-Tactile Afferents in Pain Inhibition and Tactile Allodynia. Affective Touch and the Neurophysiology of CT Afferents, 409–420. 10.1007/978-1-4939-6418-5_24.
45. Sandkühler J (2009). Models and Mechanisms of Hyperalgesia and Allodynia. Physiological Reviews 89, 707–758. 10.1152/physrev.00025.2008. [PubMed: 19342617]
46. International Association for the Study of Pain. Research Symposium, and Handwerker, H.O. (2004). Hyperalgesia: Molecular Mechanisms and Clinical Implications (International Assn for the Study of Pain).
47. Löken LS, Duff EP, and Tracey I (2017). Low-threshold mechanoreceptors play a frequency-dependent dual role in subjective ratings of mechanical allodynia. J. Neurophysiol 118, 3360–3369. [PubMed: 28954896]
48. Koltzenburg M, Lundberg LER, and Torebjörk EH (1992). Dynamic and static components of mechanical hyperalgesia in human hairy skin. Pain 51, 207–219. [PubMed: 1484717]
49. Deuis JR, Dvorakova LS, and Vetter I (2017). Methods Used to Evaluate Pain Behaviors in Rodents. Front. Mol. Neurosci 10, 284. [PubMed: 28932184]
50. Yalcin I, Charlet A, Freund-Mercier M-J, Barrot M, and Poisbeau P (2009). Differentiating thermal allodynia and hyperalgesia using dynamic hot and cold plate in rodents. J. Pain 10, 767–773. [PubMed: 19409860]
51. Schwartz ES, Lee I, Chung K, and Mo Chung J (2008). Oxidative stress in the spinal cord is an important contributor in capsaicin-induced mechanical secondary hyperalgesia in mice. Pain 138, 514–524. [PubMed: 18375065]
52. Torebjörk HE, Lundberg LE, and LaMotte RH (1992). Central changes in processing of mechanoreceptive input in capsaicin-induced secondary hyperalgesia in humans. J. Physiol 448, 765–780. [PubMed: 1593489]
53. Ziegler EA, Magerl W, Meyer RA, and Treede RD (1999). Secondary hyperalgesia to punctate mechanical stimuli. Central sensitization to A-fibre nociceptor input. Brain 122 (Pt 12), 2245–2257. [PubMed: 10581220]
54. Schuelert N, and McDougall JJ (2012). Involvement of Nav 1.8 sodium ion channels in the transduction of mechanical pain in a rodent model of osteoarthritis. Arthritis Research & Therapy 14, R5. 10.1186/ar3553. [PubMed: 22225591]
55. Niibori M, Kudo Y, Hayakawa T, Ikoma-Seki K, Kawamata R, Sato A, and Mizumura K (2020). Mechanism of aspirin-induced inhibition on the secondary hyperalgesia in osteoarthritis model rats. Heliyon 6, e03963. [PubMed: 32478188]
56. Andrew D, and Greenspan JD (1999). Mechanical and Heat Sensitization of Cutaneous Nociceptors After Peripheral Inflammation in The Rat. Journal of Neurophysiology 82, 2649–2656. 10.1152/jn.1999.82.5.2649. [PubMed: 10561434]
57. Ballantyne J (2009). Opioid Tolerance, Dependence and Hyperalgesia. Opioid-Induced Hyperalgesia, 61–73. 10.3109/9781420089004-6.
58. Abdus-Saboor I, Fried NT, Lay M, Burdge J, Swanson K, Fischer R, Jones J, Dong P, Cai W, Guo X, et al. (2019). Development of a Mouse Pain Scale Using Sub-second Behavioral Mapping and Statistical Modeling. Cell Rep. 28, 1623–1634.e4. [PubMed: 31390574]
59. Lindsay NM, Chen C, Gilam G, Mackey S, and Scherrer G (2021). Brain circuits for pain and its treatment. Science Translational Medicine 13. 10.1126/scitranslmed.abj7360.
60. Mogil JS (2009). Animal models of pain: progress and challenges. Nat. Rev. Neurosci 10, 283–294. [PubMed: 19259101]
61. Mogil JS (2012). The etiology and symptomatology of spontaneous pain. J. Pain 13, 932–933; discussion 934–935. [PubMed: 23031393]

62. Corbett DB, Simon CB, Manini TM, George SZ, Riley JL 3rd, and Fillingim RB (2019). Movement-evoked pain: transforming the way we understand and measure pain. Pain 160, 757–761. [PubMed: 30371555]
63. Mathews KA (2002). Non-steroidal anti-inflammatory analgesics: a review of current practice. Journal of Veterinary Emergency and Critical Care 12, 89–97. 10.1046/j.1435-6935.2002.00007.x.
64. Olson ME, Ralston B, Burwash L, Matheson-Bird H, and Allan ND (2016). Efficacy of oral meloxicam suspension for prevention of pain and inflammation following band and surgical castration in calves. BMC Vet. Res 12, 102. [PubMed: 27295955]
65. Bennett TE, Pavek TJ, Schwark WS, and Singh B (2021). Comparison of Nociceptive Effects of Buprenorphine, Firocoxib, and Meloxicam in a Plantar Incision Model in Sprague-Dawley Rats. J. Am. Assoc. Lab. Anim. Sci 60, 539–548. [PubMed: 34266519]
66. Ruel HLM, Watanabe R, Evangelista MC, Beauchamp G, Auger J-P, Segura M, and Steagall PV (2020). Pain burden, sensory profile and inflammatory cytokines of dogs with naturally-occurring neuropathic pain treated with gabapentin alone or with meloxicam. PLoS One 15, e0237121. [PubMed: 33253197]
67. Tomacheuski RM, Taffarel MO, Cardoso GS, Derussi AAP, Ferrante M, Volpato R, and Luna SPL (2020). Postoperative Analgesic Effects of Laserpuncture and Meloxicam in Bitches Submitted to Ovariohysterectomy. Vet. Sci. China 7. 10.3390/vetsci7030094.
68. Fudge JM, Page B, and Lee I (2021). Evaluation of Targeted Bupivacaine, Bupivacaine-lidocaine-epinephrine, Dexamethasone, and Meloxicam for Reducing Acute Postoperative Pain in Cats Undergoing Routine Ovariohysterectomy. Top. Companion Anim. Med 45, 100564. [PubMed: 34314884]
69. Hu F, Wu G, Zhao Q, and Wu J (2021). Evaluation of analgesic effect, joint function recovery and safety of meloxicam in knee osteoarthritis patients who receive total knee arthroplasty: A randomized, controlled, double-blind study. Medicine 100, e26873. [PubMed: 34477120]
70. Berkowitz RD, Mack RJ, and McCallum SW (2021). Meloxicam for intravenous use: review of its clinical efficacy and safety for management of postoperative pain. Pain Manag. 11, 249–258. [PubMed: 33291975]
71. Rahman W, Bauer CS, Bannister K, Vonsy J-L, Dolphin AC, and Dickenson AH (2009). Descending serotonergic facilitation and the antinociceptive effects of pregabalin in a rat model of osteoarthritic pain. Mol. Pain 5, 45. [PubMed: 19664204]
72. Liu P, Okun A, Ren J, Guo R-C, Ossipov MH, Xie J, King T, and Porreca F (2011). Ongoing pain in the MIA model of osteoarthritis. Neurosci. Lett 493, 72–75. [PubMed: 21241772]
73. Patel R, and Dickenson AH (2016). Mechanisms of the gabapentinoids and$\alpha_2\delta$-1 calcium channel subunit in neuropathic pain. Pharmacology Research & Perspectives 4, e00205. 10.1002/prp2.205. [PubMed: 27069626]
74. Patel R, and Dickenson AH (2016). Neuronal hyperexcitability in the ventral posterior thalamus of neuropathic rats: modality selective effects of pregabalin. Journal of Neurophysiology 116, 159–170. 10.1152/jn.00237.2016. [PubMed: 27098028]
75. Chincholkar M (2018). Analgesic mechanisms of gabapentinoids and effects in experimental pain models: a narrative review. Br. J. Anaesth 120, 1315–1334. [PubMed: 29793598]
76. Ogino K, Hatanaka K, Kawamura M, Ohno T, and Harada Y (2000). Meloxicam inhibits prostaglandin E(2) generation via cyclooxygenase 2 in the inflammatory site but not that via cyclooxygenase 1 in the stomach. Pharmacology 61, 244–250. [PubMed: 11093076]
77. Hirschberg J, and Manning CD (2015). Advances in natural language processing. Science 349, 261–266. [PubMed: 26185244]
78. Gharagozloo M, Amrani A, Wittingstall K, Hamilton-Wright A, and Gris D (2021). Machine Learning in Modeling of Mouse Behavior. Front. Neurosci 15, 700253. [PubMed: 34594182]
79. Le Q, and Mikolov T Distributed Representations of Sentences and Documents. Proceedings of Machine Learning Research 32, 1188–1196.
80. Mikolov T, Chen K, Corrado GS, and Dean J (2013). Efficient estimation of word representations in vector space. Computing Research Repository.
81. Türck D, Roth W, and Busch U (1996). A review of the clinical pharmacokinetics of meloxicam. Br. J. Rheumatol 35 Suppl 1, 13–16. [PubMed: 8630630]

82. Stucky CL, Gold MS, and Zhang X (2001). Mechanisms of pain. Proc. Natl. Acad. Sci. U. S. A 98, 11845–11846. [PubMed: 11562504]
83. Mogil JS (2020). Qualitative sex differences in pain processing: emerging evidence of a biased literature. Nat. Rev. Neurosci 21, 353–365. [PubMed: 32440016]
84. Renthal W, Tochitsky I, Yang L, Cheng Y-C, Li E, Kawaguchi R, Geschwind DH, and Woolf CJ (2020). Transcriptional Reprogramming of Distinct Peripheral Sensory Neuron Subtypes after Axonal Injury. Neuron 108, 128–144.e9. [PubMed: 32810432]
85. Website https://painseq.shinyapps.io/publish/.
86. Lockwood SM, Lopes DM, McMahon SB, and Dickenson AH (2019). Characterisation of peripheral and central components of the rat monoiodoacetate model of Osteoarthritis. Osteoarthritis Cartilage 27, 712–722. [PubMed: 30611904]
87. Choi S, Hachisuka J, Brett MA, Magee AR, Omori Y, Iqbal N-U-A, Zhang D, DeLisle MM, Wolfson RL, Bai L, et al. (2020). Parallel ascending spinal pathways for affective touch and pain. Nature 587, 258–263. [PubMed: 33116307]
88. Wilson TD, Valdivia S, Khan A, Ahn H-S, Adke AP, Martinez Gonzalez S, Sugimura YK, and Carrasquillo Y (2019). Dual and Opposing Functions of the Central Amygdala in the Modulation of Pain. Cell Rep. 29, 332–346.e5. [PubMed: 31597095]
89. Corder G, Ahanonu B, Grewe BF, Wang D, Schnitzer MJ, and Scherrer G (2019). An amygdalar neural ensemble that encodes the unpleasantness of pain. Science 363, 276–281. [PubMed: 30655440]
90. Han S, Soleiman MT, Soden ME, Zweifel LS, and Palmiter RD (2015). Elucidating an Affective Pain Circuit that Creates a Threat Memory. Cell 162, 363–374. [PubMed: 26186190]
91. Mogil JS (2020). The Measurement of Pain in the Laboratory Rodent. The Oxford Handbook of the Neurobiology of Pain, 27–60. 10.1093/oxfordhb/9780190860509.013.21.
92. IASP Announces Revised Definition of Pain (2020). https://www.iasp-pain.org/publications/iasp-news/iasp-announces-revised-definition-of-pain/.
93. Pereira TD, Tabris N, Matsliah A, Turner DM, Li J, Ravindranath S, Papadoyannis ES, Normand E, Deutsch DS, Wang ZY, et al. (2022). SLEAP: A deep learning system for multi-animal pose tracking. Nat. Methods 19, 486–495. [PubMed: 35379947]
94. Markowitz JE, Gillis WF, Jay M, Wood J, Harris RW, Cieszkowski R, Scott R, Brann D, Koveal D, Kula T, et al. (2023). Spontaneous behaviour is structured by reinforcement without explicit reward. Nature 614, 108–117. [PubMed: 36653449]
95. OpenAI (2023). GPT-4 Technical Report.
96. Abraham A, Pedregosa F, Eickenberg M, Gervais P, Mueller A, Kossaifi J, Gramfort A, Thirion B, and Varoquaux G (2014). Machine learning for neuroimaging with scikit-learn. Front. Neuroinform 8, 14. [PubMed: 24600388]
97. Seabold S, and Perktold J (2010). Statsmodels: Econometric and Statistical Modeling with Python. Proceedings of the Python in Science Conference. 10.25080/majora-92bf1922-011.
98. Le QV, and Mikolov T (2014). Distributed representations of sentences and documents. 10.48550/ARXIV.1405.4053.
99. Gensim: topic modelling for humans https://radimrehurek.com/gensim/models/phrases.html#gensim.models.phrases.original_scorer.

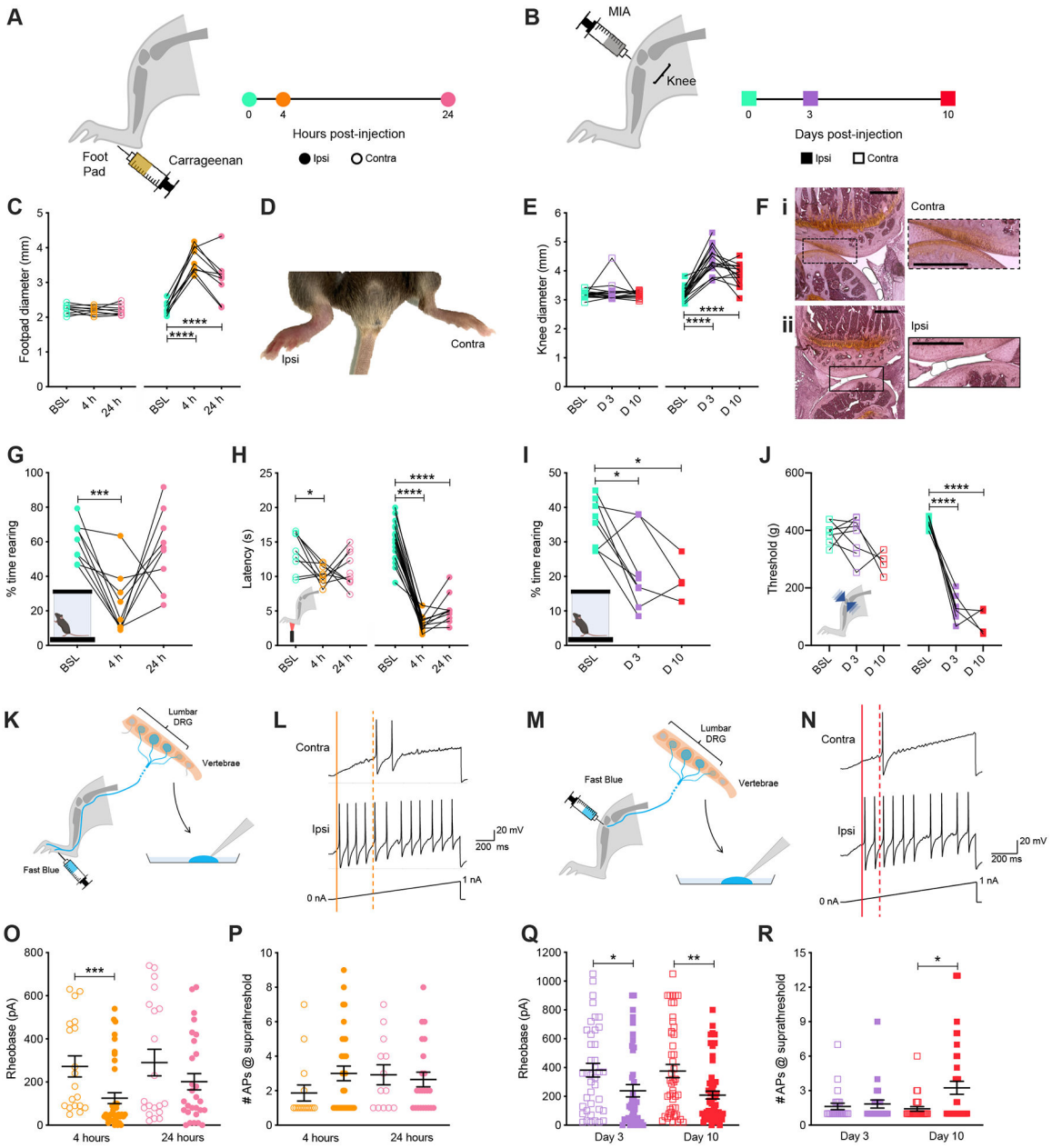


**Figure 1. Carrageenan and MIA pain models cause changes in ethological and evoked behavior accompanied by alterations in sensory neuron excitability over distinct timescales.**

Timeline of experiments following **(A)** unilateral intraplantar injection of carrageenan or **(B)** intra-articular injection of MIA. **(C)** Inflammation of the injected (Ipsi) hind paw was observed 4-hours post-injection compared to the non-injected (Contra) paw. **(D)** Footpad swelling was quantified with digital calipers following injection of carrageenan. **(E)** Histological examination of knee joints 10 days after injection showed a healthy layer of cartilage for the contralateral joint **(Ei)**, which had been lost in the ipsilateral joint **(Eii)**. **(F)** Knee joint swelling was measured following injection of MIA. **(G)** The time mice spent rearing before, 4-hours, and 24-hours post-induction of inflammation with carrageenan was assessed using a dynamic weight bearing device. **(H)** Hargreaves measurement of

carrageenan-induced heat hypersensitivity was assessed at baseline and following 4- and 24-hours. **(I)** Time spent rearing was assessed at baseline (BSL) and 3- (D 3) and 10-days (D 10) post-injection of MIA. **(J)** Sensitivity of both knee joints to mechanical stimulation was tested using a pressure application measurement device before and 3- and 10-days post-injection of MIA. **(K)** Schematic representation of retrograde labeling of hind paw innervating sensory neurons with Fast Blue followed by cell culture and whole cell patch clamp electrophysiology. **(L)** Representative current clamp recordings of Ipsi and Contra hind paw neurons of comparable capacitance, showing action potentials evoked by ramp injection of current (0–1 nA, 1 s), the thresholds for action potential discharge are annotated with dashed (Contra) or solid (Ipsi) lines. **(M)** Schematic representation of retrograde labeling of knee innervating sensory neurons with Fast Blue followed by cell culture and whole cell patch clamp electrophysiology. **(N)** Representative current clamp recordings of Ipsi and Contra knee neurons of comparable capacitance, showing action potentials evoked by ramp injection of current (0–1 nA, 1 s), the thresholds for action potential discharge are annotated with dashed (Contra) or solid (Ipsi) lines. **(O)** Step-wise current injections were used to determine the rheobase of Ipsi and Contra hind paw innervating sensory neurons 4- or 24-hours post-induction of inflammation with carrageenan. **(P)** Neurons with rheobase < 450 pA were stimulated with a suprathreshold (2 x rheobase) for 500 ms and the number of action potentials discharged counted. **(O)** Step-wise current injections were used to determine the rheobase of Ipsi and Contra knee innervating sensory neurons 3- or 10-days post-injection of MIA. **(P)** Neurons with rheobase < 450 pA were stimulated with a suprathreshold (2 x rheobase) for 500 ms and number of action potentials discharged counted. * $p < 0.05$, ** $p < 0.01$, *** $p < 0.001$, **** $p < 0.0001$: **(C, E, G, H, I, J)** one-way ANOVA with Bonferroni post hoc; **(O, Q, R)** Mann-Whitney test between Ipsi and Contra for individual time points.

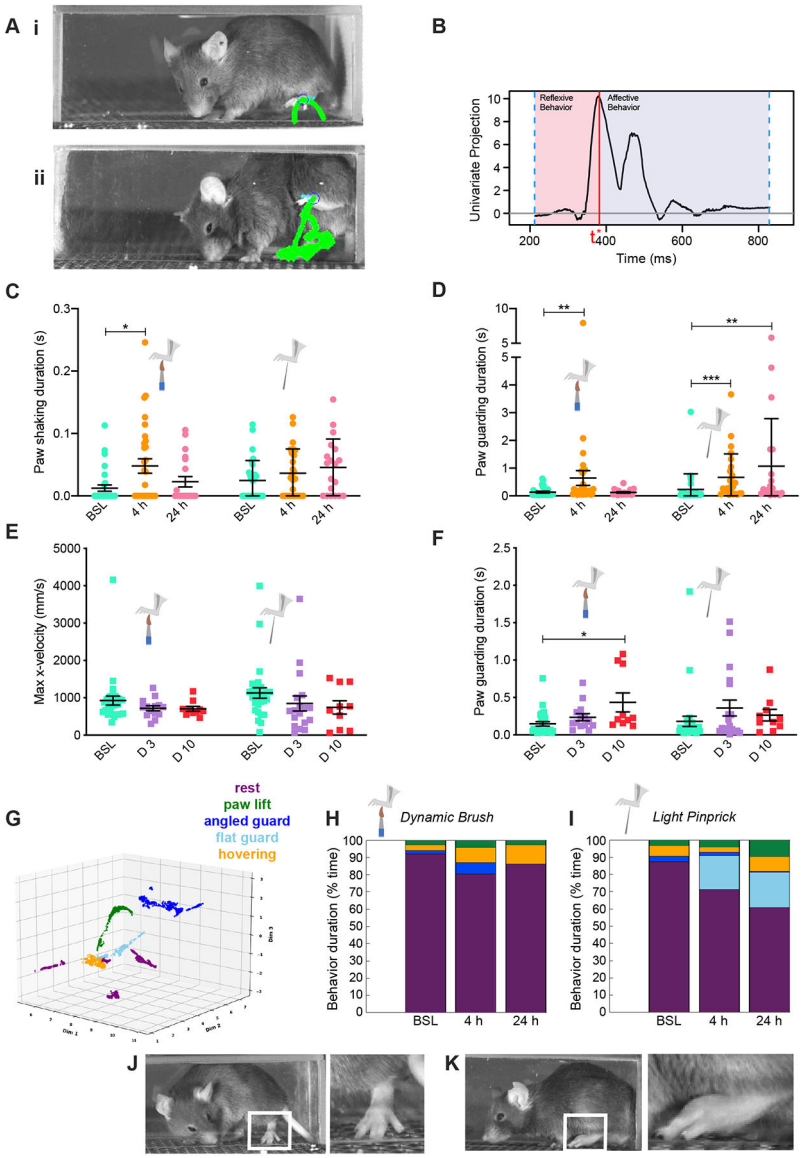


**Figure 2. PAWS and B-SOiD automated pain assessment platforms detect defensive coping behaviors associated with pain sensation during inflammation.**

**(Ai)** A behavioral response to a somatosensory stimulus at baseline. **(Aii)** Post-carrageenan injection mice guard the paw in the air for extended time. **(i,ii)** Green lines show paw trajectory pattern across entire behavior, and mouse image shows single frame with paw at its apex. **(B)** PAWS software measures reflexive (*i.e.* height, paw displacement along the y axis, etc.) and affective behavioral features (*i.e.* shaking, guarding, distance traveled by the paw, etc.). The apex t* or first peak of the behavioral response separates reflexive and affective behavioral features (as described in the methods from Jones et al., 2020). Here, the y axis is a univariate projection of the paw displacement across both x and y dimensions, in centimeters. This graph thus captures paw movements in both x and y directions over time, following dynamic brush stimulation at baseline, for 1 mouse. Further details on the computation methods used to generate this graph can be found in Jones et al., 2020. **(C,D)** Affective features such as paw guarding and paw shaking are upregulated

in response to dynamic brush and light pinprick comparing baseline to 4- and 24-hours post-carrageenan injection. **(E,F)** Paw guarding was found upregulated at 10-days after MIA knee injection, consistent with the paw being a potential secondary site of hypersensitivity. **(G)** Low-dimensional projection of feature clusters as identified after UMAP/HDBSCAN. 5 colors were then assigned to the 11 identified sub-clusters to indicate their post-hoc behavioral group assignment. Stacked bar plots of the percent of time spent doing each behavior (rest, paw lift, angled guard, flat guard, hovering) in response to dynamic brush **(H)** and **(I)** light pinprick at baseline, 4-hours, and 24-hours time points post-carrageenan injection. Responses are color-coded by the identified action type as in panel **(G)**. Examples of the angled paw guard identified by B-SOiD, which may be indicative of the activation of different subsets of sensory neurons (mechanoreceptors by brush, inducing **(J)** angled guard, nociceptors by pinprick, inducing **(K)** flat guard). N=10 mice per group; * $p < 0.05$, ** $p < 0.01$: Kruskal-Wallis test followed by Dunn's multiple comparisons were performed to determine statistical significance between the responses of mice to each stimuli across time independently.

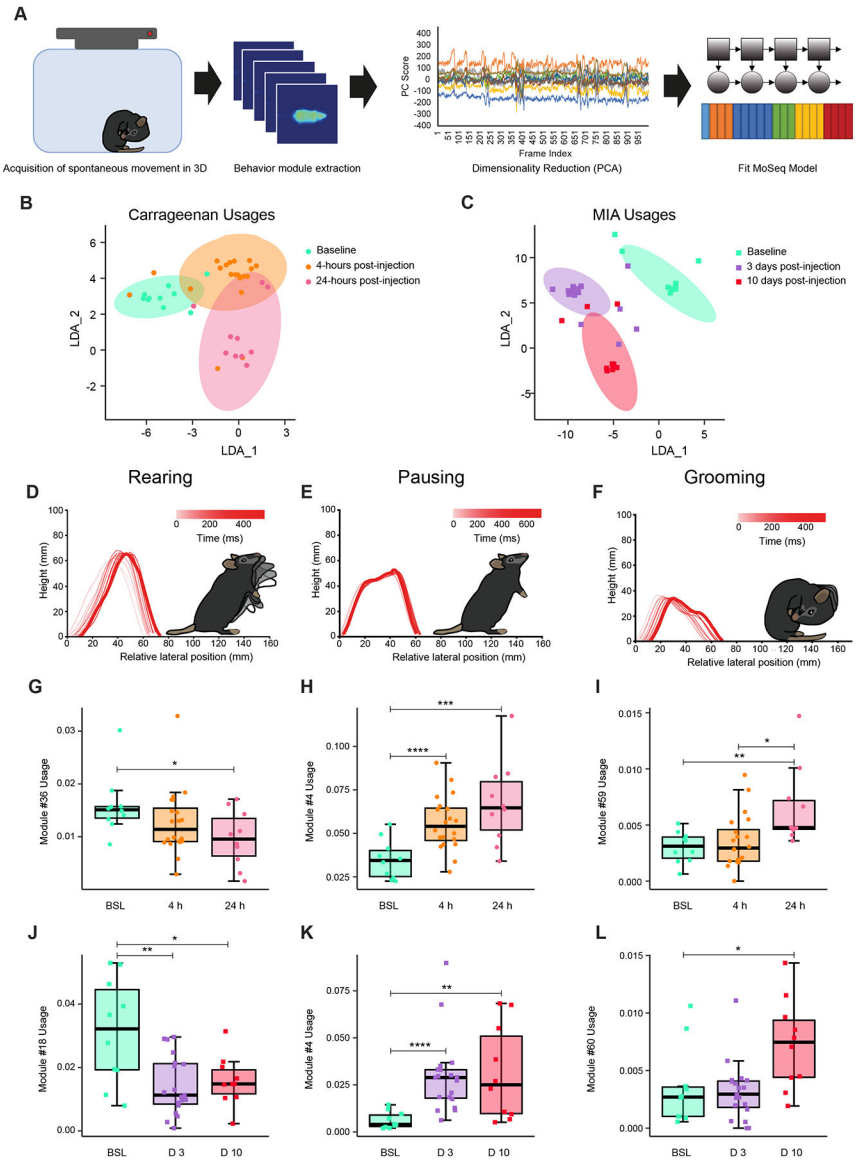


**Figure 3. 3D pose analysis detects behavioral signatures of paw carrageenan-induced inflammatory pain and knee MIA-induced injury.**

**(A)** Schematic of analysis pipeline. **(B)** Linear discriminant analysis (LDA) of spontaneous behavior module usage at baseline, and following carrageenan injection at 4- and 24-hours. **(C)** LDA of spontaneous behavior module usage at baseline, and 3- and 10-days post MIA injection. Spinogram representations of micro-movements that define particular behavioral modules identified as **(D)** rearing, **(E)** pausing and **(F)** grooming. Usage of rearing decreases following induction of inflammation with carrageenan **(G)** and MIA **(J)**. Usage of pausing **(H, K)** and grooming **(I, L)** increase following injection of carrageenan in the paw and MIA in the knee respectively. Baseline (BSL) n= 10 animals, 4h n= 20 animals, 24h n= 10 animals, D3 n= 20 animals, D10 n= 10 animals, Statistical analysis: corrected bootstrap t-test.

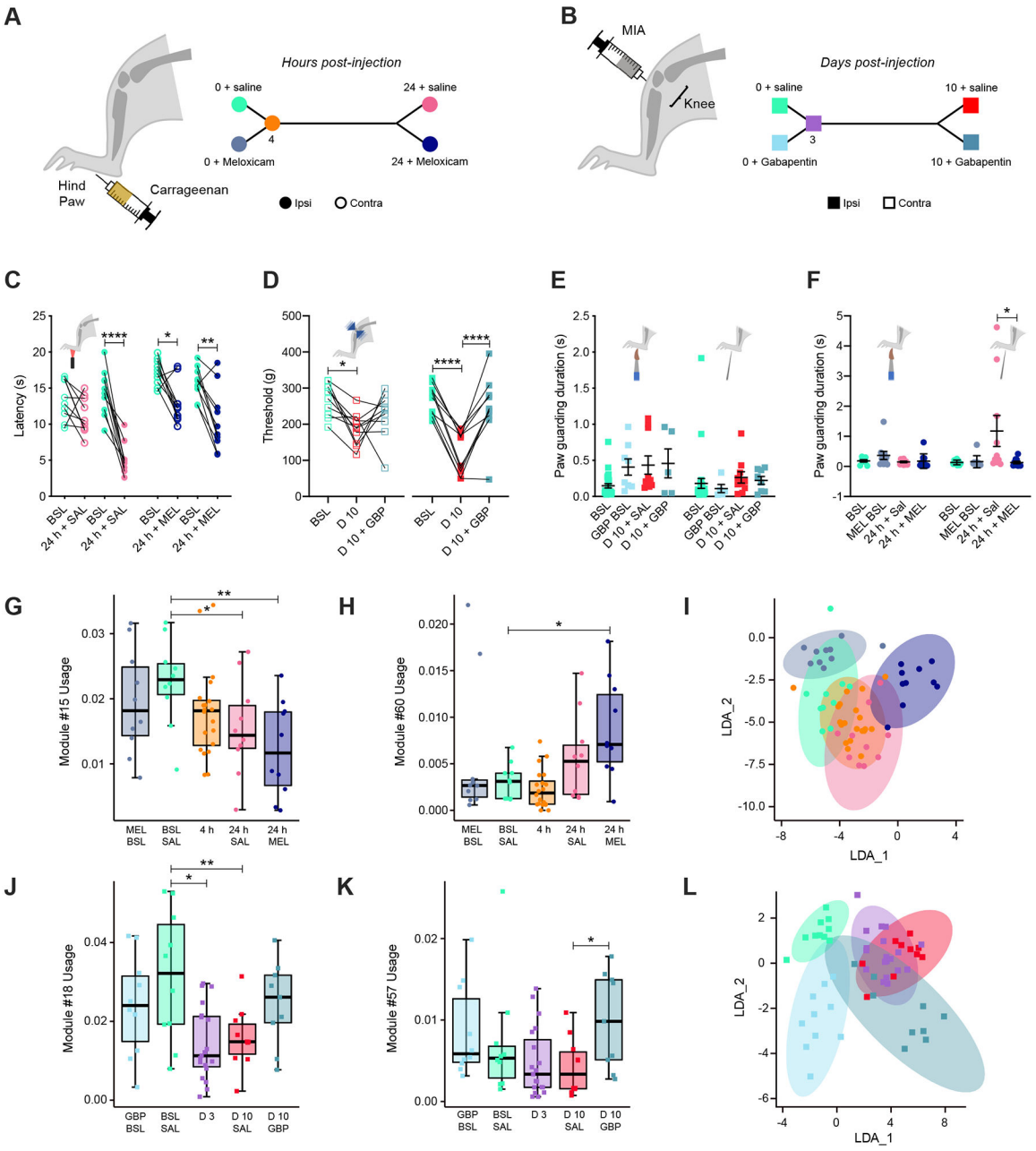


**Figure 4. Meloxicam relieves affective features of hyperalgesia but it does not promote return to pre-inflammation spontaneous behavior, while gabapentin improves spontaneous signatures of MIA-induced knee injury.**

**(A)** Timeline of the experiment. Mice were tested at baseline and after intraplantar injection of 20 µl 3% carrageenan at 4-hours post-injection, then at 24-hours after intraperitoneal injection of saline or meloxicam. **(B)** Timeline of the experiment. Mice are tested at baseline and after intra articular knee injection of 10 µl 0.1mg/ul MIA at 3-days post-injection, then at 10-days after intraperitoneal injection of saline or gabapentin. **(C)** Hargreaves measurement of carrageenan-induced heat hypersensitivity at baseline, 24-hours following carrageenan injection, as well as pain relief by meloxicam at 24-hours, ipsi- (full circles) and contralateral (empty circles) to paw injection. **(D)** Measurement of MIA-

induced pressure knee hypersensitivity at baseline, 10-days following MIA knee injection, as well as pain relief by gabapentin at 10-days, ipsi- (full squares) and contralateral (empty squares) to knee injection. **(E)** Paw guarding duration is measured with machine learning at baseline, and post-carrageenan injection at 4-hours, and 24-hours after saline or meloxicam intraperitoneal injection following dynamic brush (left) or light pinprick (right). **(F)** Paw guarding duration is measured with machine learning at baseline, and post-MIA knee injection at 3-days, and 10-days after saline or gabapentin intraperitoneal injection following dynamic brush (left) or light pinprick (right). **(G-I)** 3D pose analysis of spontaneous behavior of 5 groups: baseline + meloxicam intraperitoneal injection, baseline + saline intraperitoneal injection, 4-hours post-carrageenan paw injection, 24-hours post-carrageenan paw injection + saline intraperitoneal injection, 24-hours post-carrageenan paw injection + meloxicam intraperitoneal injection. **(G)** Spontaneous rearing behavior is decreased after paw carrageenan injection, further decreased by meloxicam intraperitoneal injection (example module #15 among other rearing modules downregulated, see Table 2). **(H)** Spontaneous grooming behavior is increased after paw carrageenan injection, further increased by meloxicam intraperitoneal injection (example module #60). **(I)** Representation of LDA of raw usage for the five different groups. **(J-L)** 3D pose analysis of spontaneous behavior 5 groups: baseline + gabapentin intraperitoneal injection, baseline + saline intraperitoneal injection, 3-days post-MIA knee injection, 10d post-MIA knee injection + saline intraperitoneal injection, 10-days post-MIA knee injection + gabapentin intraperitoneal injection. **(J)** Spontaneous rearing behavior is decreased after knee MIA injection, which can be resolved after gabapentin intraperitoneal injection (example module #18). **(K)** Locomotion is affected after knee MIA injection, which can be resolved after gabapentin intraperitoneal injection (example module #57). **(L)** Representation of LDA of raw usage for the five different groups. **(I-L)** While the point clouds in Figure 4I and 4L do show some overlap between conditions, cohorts can be distinguished by their module usage, which we quantified by computing the F1 of the LDA in predicting the condition of the held-out animals (F1-scores: CAR bsl+saline = 0.57, CAR bsl+meloxicam = 0.50, CAR 4h = 0.67, CAR 24h+saline = 0, CAR 24h+meloxicam = 0.40, overall model accuracy = 0.50 better than “pure-chance” = 0.20 and randomized data). For accuracy, we report F1, the harmonic mean of precision and recall.

For 3D pose analysis, baseline+saline (bsl+sal) n= 10 animals, baseline+meloxicam (bsl+mel) n= 10 animals, baseline+gabapentin (bsl+gbp) n= 10 animals, 4h post-carrageenan n= 20 animals, 24h post-carrageenan+saline (24h+sal) n= 10 animals, 24h post-carrageenan+meloxicam (24h+mel) n= 10 animals, D3 post-MIA n= 20 animals, D10 post-MIA+saline (D10+sal) n= 10 animals, D10 post-MIA+gabapentin (D10+gbp) n= 10 animals, Statistical analysis: corrected bootstrap t-test.

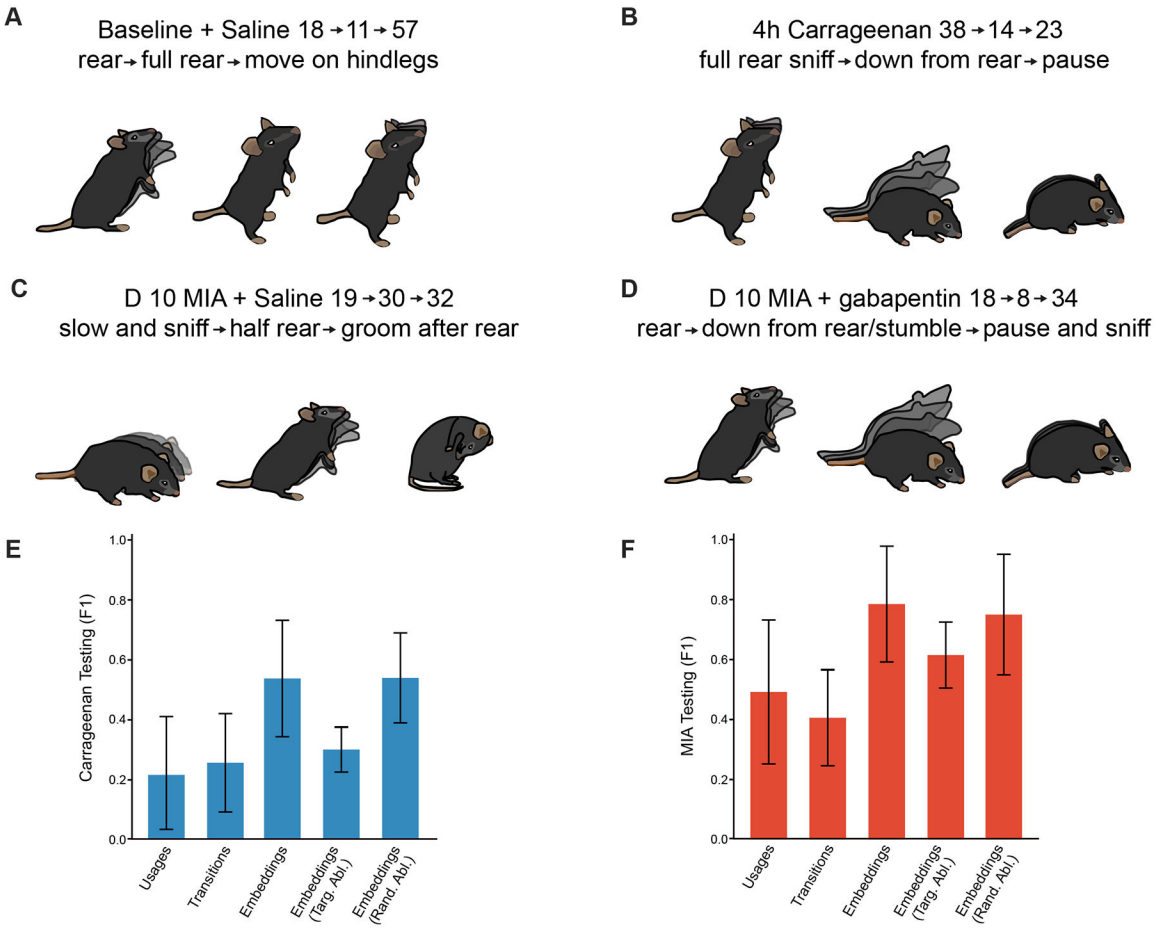


**Figure 5. Higher order behavioral sequences predict pain and analgesic states in rodents.**

**(A-D)** Example of module sequences most representative of spontaneous behavior at baseline **(A)**, 4-hours following carrageenan paw injection **(B)**, and 10-days post MIA knee injection and saline **(C)** or gabapentin **(D)** intraperitoneal injection, as identified by learned embeddings method. A standard co-location algorithm was first used to detect 2-long module sequences according to whether the 2-long sequence (e.g. A>B) appeared significantly more than each of its constituents (i.e. A or B). Wherever a significant 2-long sequence was detected, we replaced it by a new agglomerated syllable representing the co-location. We then recursed on this procedure to find 3- and 4-long sequences, at each iteration checking for the significance of agglomerated sequences by comparing their frequency to those of each of the sequence's constituents. **(E)** Bar plot showing the relative performances of the different representations along with the performance of targeted (Targ. Abl.) vs random ablations (Rand. Abl.) for carrageenan dataset. **(F)** Bar plot showing the relative performances of the different representations along with the performance of targeted (Targ. Abl.) vs random ablations (Rand. Abl.) for MIA dataset. Baseline+saline (bsl+sal) n= 10 animals, baseline+meloxicam (bsl+mel) n= 10 animals, baseline+gabapentin (bsl+gbp) n= 10 animals, 4h post-carrageenan n= 20 animals, 24h post-carrageenan+saline (24h+sal) n= 10 animals, 24h post-carrageenan+meloxicam (24h+mel) n= 10 animals, D3 post-MIA

n= 20 animals, D10 post-MIA+saline (D10+sal) n= 10 animals, D10 post-MIA+gabapentin (D10+gbp) n= 10 animals, Statistical analysis: corrected bootstrap t-test.

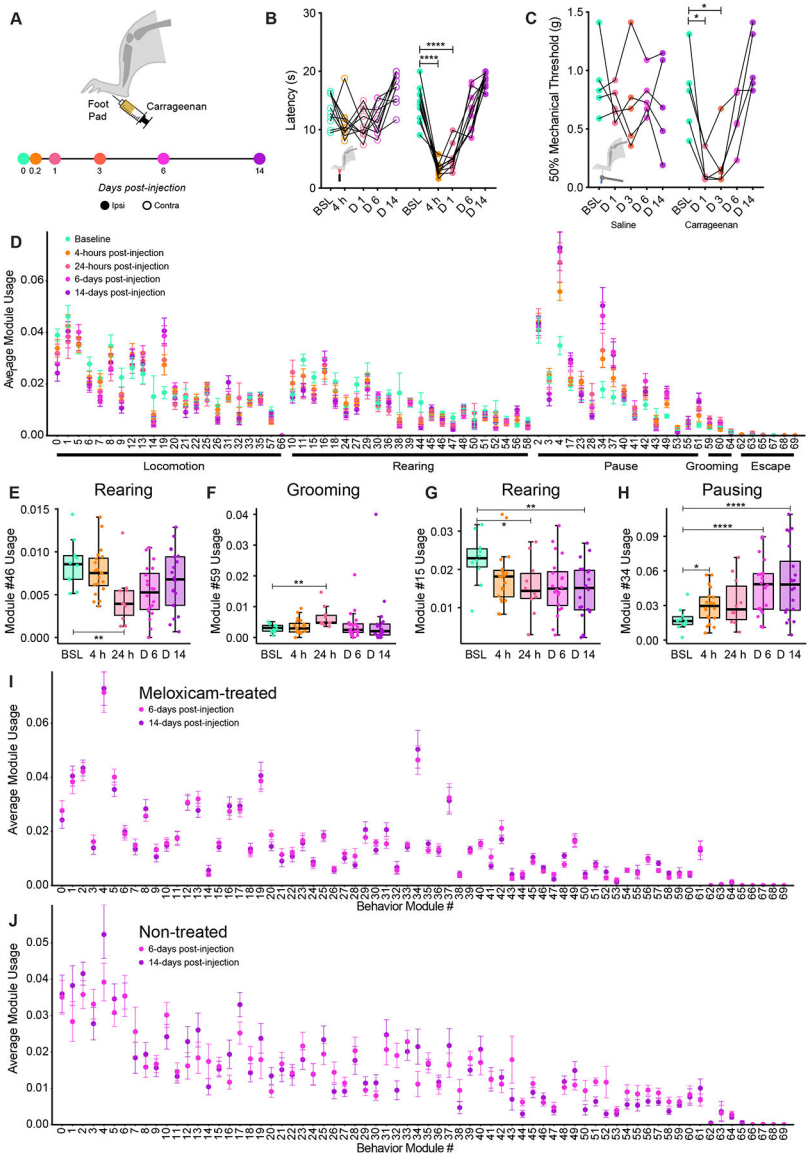


**Figure 6. 3D pose analysis resolves the behavior of animals following resolution of inflammation as a new state as opposed to return to baseline, this state is stabilized by treatment with the anti-inflammatory Meloxicam.**

**(A)** Timeline of extended behavioral characterization following induction of inflammation with carrageenan. **(B)** Heat hypersensitivity of the Ipsi paw is comparable to baseline by 6-days post-injection of carrageenan. **(C)** Intraplantar injection of saline does not affect mechanical sensitivity of the hind paw when assessed with von Frey, however, hypersensitivity is seen at 1- and 3-days post injection of carrageenan which resolves by day 6. **(D)** Mutation plot summarizing how usage of each behavioral module identified via MoSeq changes with time following intraplantar injection of carrageenan. Usage of certain behaviors including **(E)** rearing and **(F)** grooming appear to recover with time following injection of carrageenan, although others including **(G)** rearing and **(H)** pausing remain different to baseline at 14-days post-injection. **(I)** Administration of a single dose of Meloxicam at 24-hours post-injection of carrageenan stabilizes spontaneous behaviors

at time points where evoked-sensitivity has recovered. **(J)** Spontaneous behavior is more variable when tested after absence of pain relief. For 3D pose analysis, baseline+saline (bsl+sal) n= 10 animals, 4h post-carrageenan n= 20 animals, 24h post-carrageenan+saline (24h+sal) n= 10 animals, 6d post-carrageenan n= 20 animals, 14d post-carrageenan n= 20 animals, Statistical analysis: corrected bootstrap t-test.

**Table 1.**

Electrophysiological characterization of cultured neurons innervating the inflamed paw reveal unique cellular signatures that punctuate the pain progression at 4- and 24-hours.

| | Hours post-inflammation | | | |
|---|---|---|---|---|
| | 4 hours | | 24 hours | |
| | Contra (n = 22) | Ipsi (n = 39) | Contra (n = 20) | Ipsi (n = 30) |
| Resting membrane potential (mV) | −47.27 ± 1.56 * | −43.38 ± 0.90 * | −46.95 ± 1.52 | −44.70 ± 1.38 |
| Capacitance (pF) | 31.23 ± 2.69 | 25.90 ± 1.73 | 30.77 ± 4.44 | 33.17 ± 3.03 |
| Action potential amplitude (mV) | 80.33 ± 3.95 | 84.58 ± 2.17 | 85.45 ± 3.65 | 87.11 ± 2.74 |
| Half peak duration (ms) | 3.04 ± 0.26 | 3.50 ± 0.15 | 3.87 ± 0.35 | 3.37 ± 0.27 |
| Afterhyperpolarization amplitude (mV) | 15.43 ± 1.30 | 14.10 ± 0.76 | 16.61 ± 0.71 | 16.15 ± 0.84 |
| Afterhyperpolarization duration (ms) | 15.36 ± 1.55 | 17.82 ± 1.55 | 15.48 ± 1.17 | 16.45 ± 1.19 |

Intrinsic and active properties of hind paw innervating dorsal root ganglion neurons from the carrageenan injected side (Ipsi) and contralateral (Contra) side.

* $p < 0.05$, unpaired t-test.

**Table 2.**

Electrophysiological characterization of cultured neurons innervating the injured knee reveal unique cellular signatures that punctuate the pain progression at Day 3 and Day 10.

| | Days post-injection | | | |
|---|---|---|---|---|
| | Day 3 | | Day 10 | |
| | Contra (n = 40) | Ipsi (n = 42) | Contra (n = 48) | Ipsi (n = 57) |
| Resting membrane potential (mV) | −45.93 ± 0.88 | −43.07 ± 1.18 | −48.04 ± 1.18 *** | −42.35 ± 1.00 *** |
| Capacitance (pF) | 38.72 ± 3.04 | 38.65 ± 3.43 | 40.23 ± 3.48 | 42.75 ± 3.18 |
| Action potential amplitude (mV) | 86.83 ± 2.74 | 78.73 ± 0.24 | 85.98 ± 3.03 | 85.15 ± 2.66 |
| Half peak duration (ms) | 2.29 ± 0.16 | 2.77 ± 0.24 | 2.19 ± 0.17 | 2.60 + 0.14 |
| Afterhyperpolarization amplitude (mV) | 15.66 ± 0.65 | 14.69 ± 0.68 | 14.63 ± 0.78 | 14.77 ± 0.77 |
| Afterhyperpolarization duration (ms) | 9.50 ± 0.66 | 8.17 ± 0.56 | 11.71 ± 1.20 | 12.17 ± 1.14 |

Intrinsic and active properties of knee innervating dorsal root ganglion neurons from the MIA injected side (Ipsi) and contralateral (Contra) side.

*** $p < 0.001$, unpaired t-test.

## Key resources table

| REAGENT or RESOURCE | SOURCE | IDENTIFIER |
|---|---|---|
| Antibodies | | |
| Anti-TRPV1 Guinea Pig (polyclonal) | Alomone | Cat#:ACC-030-GP RRID:AB_2721813 |
| Anti-Guinea Pig IgG (Alexa Fluor 488 conjugated) | Jackson ImmunoResearch | Cat#:706-545-148 RRID:AB_2340472 |
| Chemicals, peptides, and recombinant proteins | | |
| Fast Blue | Polysciences | Cat#:17740 |
| λ-carrageenan (Rutgers - Cambridge - Columbia) | Sigma-Aldrich | Cat#:22049 |
| Monosodium iodoacetate (Cambridge) | Sigma-Aldrich | Cat#:I2512 |
| Gabapentin (Rutgers - Cambridge) | Sigma-Aldrich | Cat#:1287303 |
| Monosodium iodoacetate (Rutgers - Columbia) | VWR | Cat#:200006-706 |
| Meloxicam | covetrus | Cat#:049755 |
| Deposited data | | |
| Study Data | This study | Zenodo: https://doi.org/10.5281/zenodo.7884191 |
| Experimental models: Organisms/strains | | |
| C57BL/6J mice (Cambridge) | Envigo | Wild-type |
| C57BL/6N mice (Rutgers) | Charles River | Wild-type |
| C57BL/6 (Columbia) | Jackson Laboratories | Wild-type |
| Software and algorithms | | |
| Patchmaster | HEKA | heka.com |
| Fitmaster | HEKA | heka.com |
| Igor pro | WaveMetrics | wavemetrics.com |
| Patcher's Power Tools | Max-Planck-Institut | www3.mpibpc.mpg.de/groups/neher/index.php?page=aboutppt |
| R Studio | R | rstudio.com/products/rstudio |
| Fiji | ImageJ | imagej.net/software/fiji/ |
| μManager | NIH | micro-manager.org |
| DWB2 | Bioseb | bioseb.com |
| Python | Python Software Company | RRID:SCR_008394 |
| MoSeq | Wiltschko et al.[26] | dattalab.github.io/moseq2-website/index.html |
| moseq2-lda | This study | github.com/tischfieldlab/moseq2-lda |
| moseq2-nlp | This study | github.com/tischfieldlab/moseq2-nlp |
| moseq-reports | This study | github.com/tischfieldlab/moseq-reports |
| Gensim | Radim Rehurek, Petr Sojka. Software framework for topic modeling with large corpora. 2010. THE LREC 2010 WORKSHOP ON NEW CHALLENGES FOR NLP FRAMEWORKS. Pg. 45–50. University of Malta | github.com/RaRe-Technologies/gensim |
| PAWS | Jones et al.[21] | github.com/crtwomey/paws |

| REAGENT or RESOURCE | SOURCE | IDENTIFIER |
|---|---|---|
| B-SOiD | Hsu et al.[23] | github.com/YttriLab/B-SOID |
| DeepLabCut | Mathis et al.[22] | github.com/DeepLabCut/DeepLabCut |
| Proanalyst | Xcitex Inc. | xcitex.com/proanalyst-motion-analysis-software.php |
| Other | | |
| Kinect2 | Microsoft | amazon.com/kinect-v2/s?k=kinect+v2 |
| Open-field assay enclosure | US Plastics | usplastic.com/catalog/item.aspx?itemid=120721 |